FIFTH QUARTERLY REPORT

FOR

A DAY-NIGHT HIGH RESOLUTION INFRARED

RADIOMETER EMPLOYING TWO-STAGE RADIANT COOLING

(1 April 1967 - 1 July 1967)

Contract No. NAS 5-10113

Prepared by

ITT Industrial Laboratories
Fort Wayne, Indiana 46803

For

National Aeronautics and Space Administration
Goddard Space Flight Center
Greenbelt, Maryland 20771

ITTIL No. 67-1035 15 July 1967

FIFTH QUARTERLY REPORT

FOR

A DAY-NIGHT HIGH RESOLUTION INFRARED RADIOMETER EMPLOYING TWO-STAGE RADIANT COOLING

(1 April 1967 - 1 July 1967)

Contract No. NAS 5-10113

Prepared by

ITT Industrial Laboratories
Fort Wayne, Indiana 46803

For

National Aeronautics and Space Administrations
Goddard Space Flight Center
Greenbelt, Maryland 20771

Contributors

R. V. Annable, J. F. Lodder,
R. A. Harber, W. H. Wallschlaeger, G. Eiden

Approved by

K. L. DeBrosse, Manager
Space & Applied Science Dept.

Dr. C. W. Steeg Jr., Director
Product Development

Dr. R. T. Watson, President
ITT Industrial Laboratories

ABSTRACT

This report describes the initial testing of a two-stage radiant cooler to be used in a 10.5 to 12.5 micron Day-Night High Resolution Infrared Radiometer and outlines the initial electronic design of a breadboard radiometer. A complete two-stage patch assembly passed sinusoidal vibration tests at Nimbus prototype levels. Thermal tests on single-stage models of the radiant cooler showed that evaporation of aluminum and gold on Alzak treated aluminum does not produce a suitable cone surface, while aluminized mylar produces a cone surface whose emissivity is within the design range (0.086 to 0.02). The average cone surface emissivity including support and optical openings is 0.063 in the cooler employing aluminized mylar; this corresponds to an in-orbit patch temperature of 98 degrees K in a single-stage cooler. The helium refrigerator and attached copper structure used to simulate cold space during cooler tests operated close to design values following modification of the support and coupling of the refrigerator. The status of the electronic test equipment is given and the design of the relay optics is outlined. Finally, the initial design of the radiometer electronics is covered.

TABLE OF CONTENTS

LIST OF ILLUSTRATIONS

LIST OF TABLES

1.0 INTRODUCTION

This report covers the technical aspects of the work performed in the development of a two-stage radiant cooler and associated 10.5 to 12.5 micron day-night radiometer during the quarterly period from 1 April 1967 to 1 July 1967. During the reporting period, a complete two-stage patch assembly passed sinusoidal vibration tests at Nimbus prototype levels. The remaining instruments for the electronic test equipment were selected, and the support and coupling of the helium refrigerator were modified. Testing of the helium refrigerator and attached copper structure and aluminum shroud showed that the cold space simulator operates close to its design values. Thermal tests on single-stage radiant cooler showed that a cone surface of Alzak treated aluminum covered with evaporated aluminum and evaporated gold has too high an emissivity (0.20). On the other hand, a cone surface of aluminized mylar has an emissivity of 0.063, which corresponds to an in-orbit patch temperature of 98 degrees K in a single-stage cooler. The optical design of the breadboard radiometer was completed and the electronic design begun.

A 10.5 to 12.5 micron instrument permits radiometric mapping of the earth and its cloud cover both day and night. It is an extension of the 3.4 to 4.2 micron nighttime High Resolution Infrared Radiometer flown on Nimbus I and II. The two-stage radiant cooler is an extension of the single-stage cooler employed on the Nimbus radiometer.

This report is for the fourth quarter of the second phase of the program, which was initiated following approval of the First Quarterly (Design Study) Report. The second phase is the construction and testing of a vibrationally sound two-stage cooler, with the objective of attaining a temperature below 80 degrees K. The third phase is the integration of the radiant cooler with a working breadboard radiometer of specific characteristics.

2.0 VIBRATION TESTS

A patch assembly for the two-stage radiant cooler (Third Quarterly Report, Figure 4) was subjected to a sinusoidal vibration test on May 8 and 9. The purpose of this test was to determine if the support mechanisms of an integrated patch assembly could sustain the same vibration levels as those imposed on Nimbus prototype instruments. The first-stage patch was held by a caging mechanism consisting of removable pins (Second Quarterly Report, Section 3.4). The number of pins was increased from three to four, and an in-orbit support tube (1/4 inch OD, 1/16 inch ID) was attached to both ends of the first-stage patch.

The assembly was first vibrated with the smaller, second-stage patch removed. After vibrating in all three planes from 0 to 2000 cps at 10 g and then at 20 g, the patch and supports were found to be free of any damage. During the 20 g vibration some small deflection waves were observed at the end of the second stage cones through the 80 to 170 cps range.

The patch was then reassembled with the smaller, or second-stage patch in place and aligned with respect to the optical axis. This integrated patch was then vibrated as above, first at 10 g and then at 20 g. Through the frequency range of 75 to 135 cps the small patch became unstable and the deflection reached approximately 1/8 inch at 20 g when vibrated in the plane perpendicular to the throat of the cone (i.e. along the cone axis). After the tests were completed the patch assembly was inspected and no parts were found to be damaged or to have shifted from their initial positions. The test report is reproduced on the next page.

ITT Federal Laboratories
Fort Wayne, Indiana
Test Laboratory

No. 1197 Procedure Report May 10, 1967

1.0 Description

1.1 One (1) patch assembly, manufactured by ITT Industrial Laboratories, was submitted for test. The patch assembly part number is D-4710251.

2.0 Procedure

2.0 The patch assembly was mounted on the vibration machine in an ITT Industrial Laboratories supplied fixture and subjected to a harmonic motion along each of three mutually perpendicular axes. One sweep in each of the three mutually perpendicular planes was at an acceleration level of 1/4 inch DA or 10 g's whichever is less. One sweep in each of the three mutually perpendicular planes was at an acceleration level of 1/4 inch DA or 20 g's whichever is less except in the frequency range of 40 to 500 cps where the level was 17 g's. The total frequency range of 5 cps to 2000 cps was swept at rates so that the ranges 5 to 100 cps, 100 cps to 500 cps and 500 cps to 2000 cps were traversed in approximately 3.25 minutes, 2.75 minutes and 2.56 minutes respectively for a total sweep time of approximately 8.56 minutes.

2.1.1 The above procedure was repeated after the installation of the secondary patch or otherwise known as the small patch.

3.0 Results

3.1 The patch assembly was mounted in the vibration fixture and observed during the vibration tests by Mr. J. Lodder of ITT Industrial Laboratories.

3.2 No visible damage was noted during the vibration tests.

4.0 Notes

4.1 The test was requested by Mr. J. Lodder.

4.2 The test was completed on May 9, 1967.

4.3 The vibration test was performed by L. M. Brown

3.0 TEST EQUIPMENT

The remaining parts and commercial instruments for the electronic test equipment were placed on order in preparation for the third phase of the program (breadboard radiometer). Initial operation of the helium refrigerator used to cool the space simulator showed that changes were necessary in the support and coupling of the refrigerator and space chamber.

3.1 Electronic Test Equipment

A block diagram and configuration drawing of the electronic test equipment are given in Section 4.0 of the Second Quarterly Report, which also includes material and status lists. The following list gives the current status of commercial equipment for Phase II (radiant cooler testing).

	ITEM	STATUS
1.	Honeywell Class 16 Electronik Multipoint Strip Chart Recorder	Installed in cabinet 1
2.	Low Temperature Monitor Unit; Rosemount Resistance Bridge and Sensors	Resistance bridge installed in cabinet 1; sensors on the refrigerator and space simulator
3.	HP Model 122AR Oscilloscope	Installed in cabinet 3
4.	Low Voltage High Current Power Supply, HP-6433B	Installed in cabinet 1
5.	24V DC Power Supply, Lambda LA50-03BM	Installed in cabinet 1
6.	Thermoelectric Baseplate Unit	Received

The thermoelectric baseplate unit will not be used. First, most of the breadboard electronics will be mounted in the test equipment cabinets outside the space chamber. Secondly, the baseplate makes a negligible contribution to the in-orbit thermal load on the first-stage cone, and thirdly, it is not useful for chamber simulation of the orbital thermal load on the cooler.

The status of commercial electronic test equipment for Phase III (radiometer testing) is as follows:

	ITEM	STATUS
1.	Visicorder 1508 Oscillograph	Due 7/23/67
2.	6 Channel Galvanometer Amplifier T6GA-500	Received
3.	Galvanometers for Item 1; 2 each M3300, M8000, M13000	Received
4.	Digital Voltmeter, Hewlett Packard 3460B	Received
5.	Digital Printer, Hewlett Packard HP-P76-5624R	Received

The remaining Phase III instruments are fabricated in house. Because of the minor hardware cost, most of these units were constructed during Phase II. These are the thermoelectric control unit, the blackbody target and target temperature control, the secondary voltage standard, and the motor power supply; all of them are described in Sections 4.1 through 4.4 of the Second Quarterly Report. The thermoelectric control unit will not be needed because of the removal of the thermoelectric baseplate unit. Neither will the 100 cps motor power supply, since a model 246, 1800 rpm Bodine 60 cycle motor will be used in place of the Roters motor. The Roters unit has a high cost and long delivery time and does not appear suitable for a breadboard unit. Power to the Bodine motor will be controlled by a rack-mounted variac.

The instruments remaining to be constructed are the patch panel and input scanner (See Figure 6 in the Second Quarterly Report). Parts for these units have been ordered, but fabrication has not been started.

3.2 Modification of Refrigerator Support and Coupling

The first approach to mating the helium refrigerator (cryogenerator) to the space chamber by using a platform on screw jacks (First Quarterly Report, Figure 16; Third Quarterly Report, Figure 7; Fourth Quarterly Report, Figures 5, 7, 8) proved to be unstable during operation. A more rigid attachment of the space chamber and cryogenerator to the floor was needed along with a flexible flange coupling between the cryogenerator and chamber to prevent excessive loading on the cryogenerator. Figure 1 shows the new mating arrangement; the chamber and cryogenerator are tied to the floor by steel beams, and the flexible coupling is provided by a stainless steel bellows with a spring rate of approximately 200 pounds per inch. The bellows assembly is shown in detail in Figure 2 together with the cryogenerator attachments for the copper cold target and aluminum shroud. The modified attachment and support permitted stable operation of the cryogenerator and proper cooling of the copper and aluminum (see Section 4.3). The equipment has been successfully operated for a total period of about 90 hours.

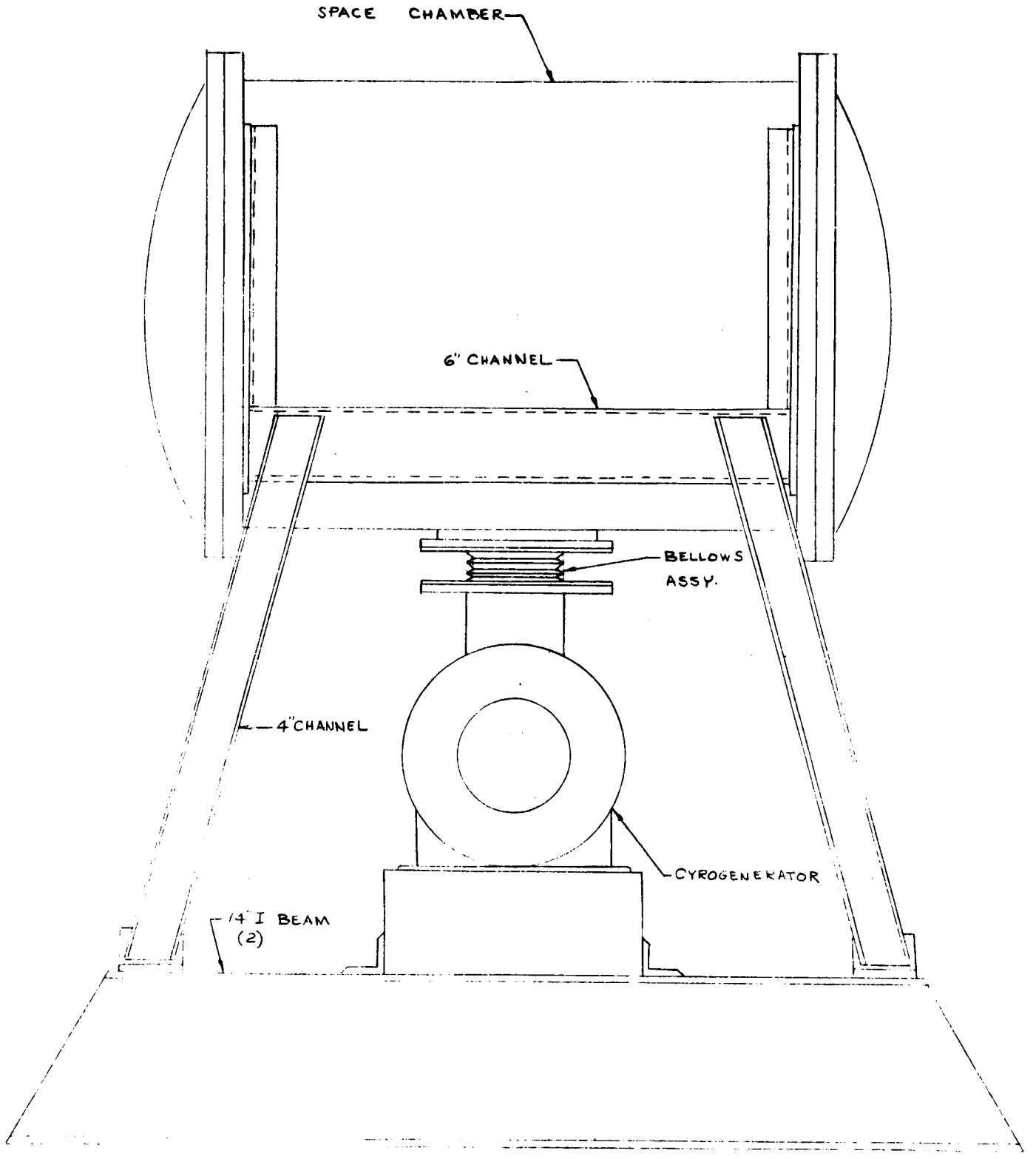

Figure 1 Space Chamber and Cryogenerator Support and Coupling

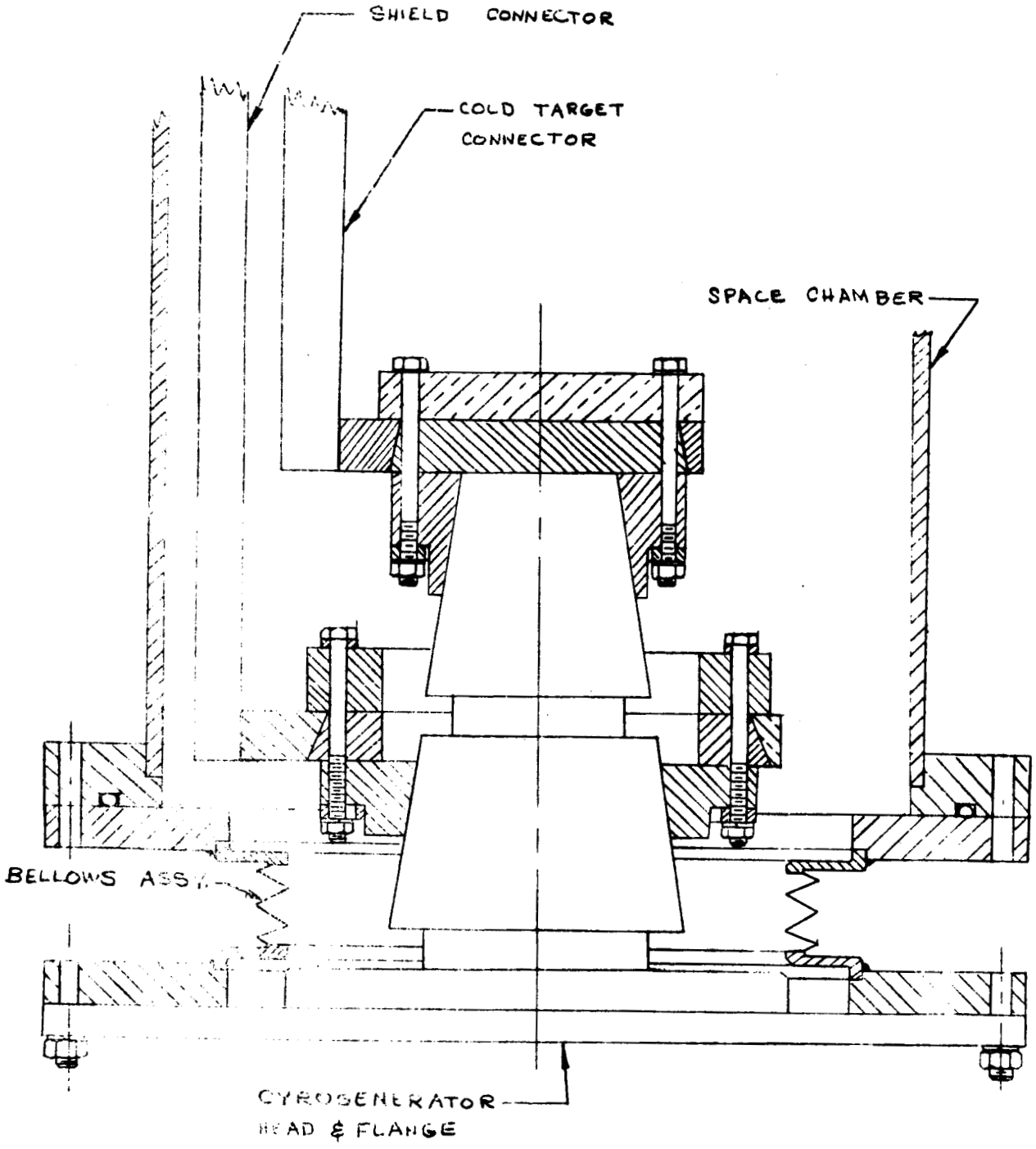

Figure 2 Flexible Coupling, Cryogenerator to Space Chamber

4.0 THERMAL TESTS

The performances of two single-stage models of the two-stage radiant cooler were determined by means of the thermal-vacuum test equipment (Fourth Quarterly Report, Section 3.0) and temperature measuring instruments (First Quarterly Report, Section 5.2; Second Quarterly Report, Section 4.0). The final equilibrium temperatures were used to calculate the effective patch-to-cone emissivity (First Quarterly Report, Section 5.4) and the effective emissivity between the outer box and first-stage cone (Second Quarterly Report, Section 5.5.1). The average emissivity of the cone surface can be determined from the effective patch-to-cone emissivity and the cone geometry (First Quarterly Report, Appendix III; Fourth Quarterly Report, Section 4.3). The in-chamber temperature of the cone, and therefore the accuracy of simulating in-orbit operation, is determined by the box-cone emissivity and the temperature of the outer box together with the cone surface emissivity and cooler geometry.

The first cooler to be tested has a cone surface of Alzak treated aluminum covered with successive layers of evaporated aluminum and gold. Its cone surface emissivity is 0.20 (Section 4.2), which is considerably above the design range of 0.086 to 0.02. The surface emissivity is an average value and assumes specular reflection at the cone walls and a black patch; it includes the openings for the in-orbit support tubes and optics as well as the small conductive coupling through the in-orbit support tubes (Second Quarterly Report, Section 5.3).

Much better results were obtained with the second cooler to be tested, which has a cone surface of aluminized mylar. Its cone surface emissivity is 0.063 (Section 4.2), which corresponds to an in-orbit patch temperature of about 98 degrees K in a single-stage cooler for an orbit normal to sun angle of 79 degrees (Section 4.2). The ratio of patch temperature to cone temperature was 0.48 in the second cooler compared with 0.64 in the first.

The first-stage cone and patch in the aluminized mylar model attained temperatures about 10 percent below their expected orbital values (Section 4.3). The thermal load on the cone will be increased in future tests to increase the accuracy of thermal simulation.

The helium refrigerator and attached copper and aluminum structures provided a cold space reference suitable for thermal testing of the radiant coolers (Section 4.4).

The residual gas pressure in the space chamber during the second and third thermal tests reached levels at which gas conduction is entirely negligible (Section 4.5).

A non-black space reference reflects part of the patch and cone radiation back to the patch, thus increasing the patch temperature. The temperature of a black patch is about 4.2 percent higher when the reference has a diffuse reflectivity of 5 percent (Section 4.6).

4.1 Single-Stage Cooler Models

Three thermal tests were conducted on single-stage models of the two-stage radiant cooler. The first two tests were on a cooler with an Alzak cone surface covered with evaporated aluminum and gold. The third test was on a cooler with a cone surface covered with aluminized mylar. Patches in both coolers were painted with 3M Black Velvet and were supported at two ends by Synthane G-10 (in-orbit) support tubes of 1/4-inch outside diameter and 3/16-inch inside diameter. The support tubes were not covered with evaporated gold or wrapped with multilayer insulation (See Second Quarterly Report, Section 5.3). However, the radiative coupling to the surfaces of the tubes was reduced by concentric cylindrical inserts mounted to the patch and covered on their inner surfaces with evaporated gold (See First Quarterly Report, Figure 13). In addition to the openings through the cone wall for the support tubes, openings were provided for the optical beam and the four patch caging pins.

Temperature measurements during the first radiant cooler test are shown in Figure 3. Time is measured from the start of the A-20 helium refrigerator. The temperatures of the outer box, cone, and patch were measured by means of chromel-alumel thermocouples. The cone temperature was measured near its ends and at the frame in the center. There was a 3 to 4 degree K temperature difference from either end to the center of the cone. After about 12 or 13 hours the regular decrease in temperatures was interrupted, as shown by the break in the curves of temperature versus time. This was probably caused by the cracking and flaking of the paint (3M Black Velvet) on the copper space reference, which was evident on removal of the cooler. Toward the end of the test run, "frost" was evident on the cold exchanger of the A-20; this appears to have been produced by air leaking into the vacuum system. After the A-20 had been turned off to allow it to warm up, large volumes of gas were given off by the cold exchangers, copper reference, and aluminum shroud.

Following completion of the first thermal test and removal of the radiant cooler, the vacuum system was restarted (the helium regrigerator was not turned on). It was evident that a leak had developed; the pressure reached only 2×10^{-4} Torr. A large leak was located in the O-ring seal of the front chamber door and a second, smaller leak in the O-ring seal of the air-release line. After repair of these leaks, the vacuum system operated satisfactorily, reaching pressure of 1.8×10^{-6} Torr after 5 hours of pumping.

The copper end plates used to simulate cold space were removed from the space chamber and cleaned of paint and primer. The plates were then sandblasted, repainted with 3M Black Velvet (no primer was used), and baked in an oven to set the paint. No cracking or flaking of the new paint surface was evident following temperatures cycles from ambient to 30 degrees K and back during the next two thermal tests.

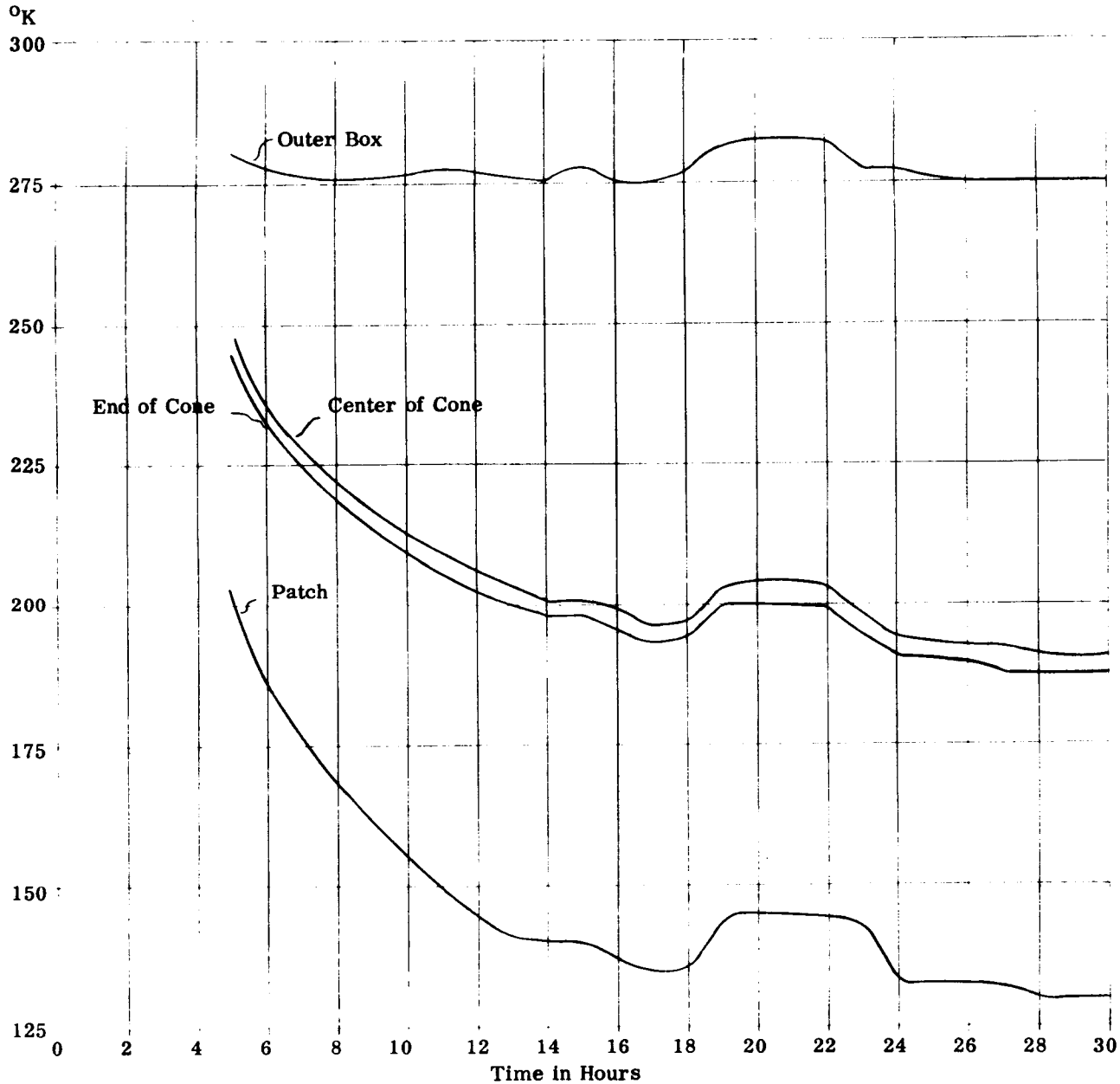

Figure 3 Radiant Cooler Test No. 1 (Au on Al on Alzak Cone)

Because of the problem with the space simulator and with vacuum leaks during the first run, a second thermal test was made on the Alzak cooler model. The results are shown in Figure 4. The patch reached a final (equilibrium) temperature of 113 degrees K with the cone at 177 degrees K (average over surface) and the outer box at 269 degrees K. Analysis of these results (Section 4. 2) showed that they are not adequate; the cone surface has an emissivity about 2. 3 times the maximum design value (0. 086).

The second single-stage cooler to be tested has a cone surface of aluminized mylar. This surface was obtained by attaching sheets of 0. 5-mil mylar covered with evaporated aluminum to the cone walls. The temperature measurements are shown in Figure 5. The patch attained an equilibrium temperature of 88 degrees K with the cone at 183 degrees K and the outer box at 279 degrees K. The patch temperature is about 10 percent below the expected in-orbit value because the thermal load on the cone was too low (Section 4. 3).

Analysis of the third thermal test showed that the cone surface in the second cooler has an emissivity of 0. 063 (Section 4. 2). The second cooler will therefore be changed to a two-stage model and used for future thermal testing. In addition, the coupling between the outer box and first-stage cone will be increased so that measured temperatures are closer to orbital values (Section 4. 3).

4. 2 Radiative Transfer Parameters

The emissivity, ϵ_g, of the surface on the first-stage cone has a large influence on the design (First Quarterly Report, Sections 4. 2 and 4. 3) and performance (Second Quarterly Report, Sections 5. 1. 3 and 5. 1. 4) of the two-stage radiant cooler. The effective emissivity, ϵ_{bc}, between the outer box and first-stage cone plus the temperature of the box determine the thermal load on the first-stage cone during thermal tests. Adjustments in the box-cone emissivity can therefore be made to increase the accuracy of simulating in-orbit thermal conditions (Section 4. 3). The value of ϵ_g can be calculated from the measured temperatures of the first-stage patch and cone and the known geometry of the cooler. The value of ϵ_{bc} can be calculated from the measured temperatures of the outer box and first-stage cone, the value of ϵ_g, and the geometry of the cooler.

The average surface emissivity of the cone walls in a radiant cooler is the solution to the equation (First Quarterly Report, Appendix III)

$$1 - \epsilon_{pc} = \frac{1}{2} \sum_{\text{Vertical}} f_n (1 - \epsilon_g)^n + \frac{1}{2} \sum_{\text{Horizontal}} f_n (1 - \epsilon_g)^n \qquad (1)$$

where ϵ_{pc} = effective patch-to-cone emissivity

f_n = view factor from patch to space as seen by n reflections in the cone walls

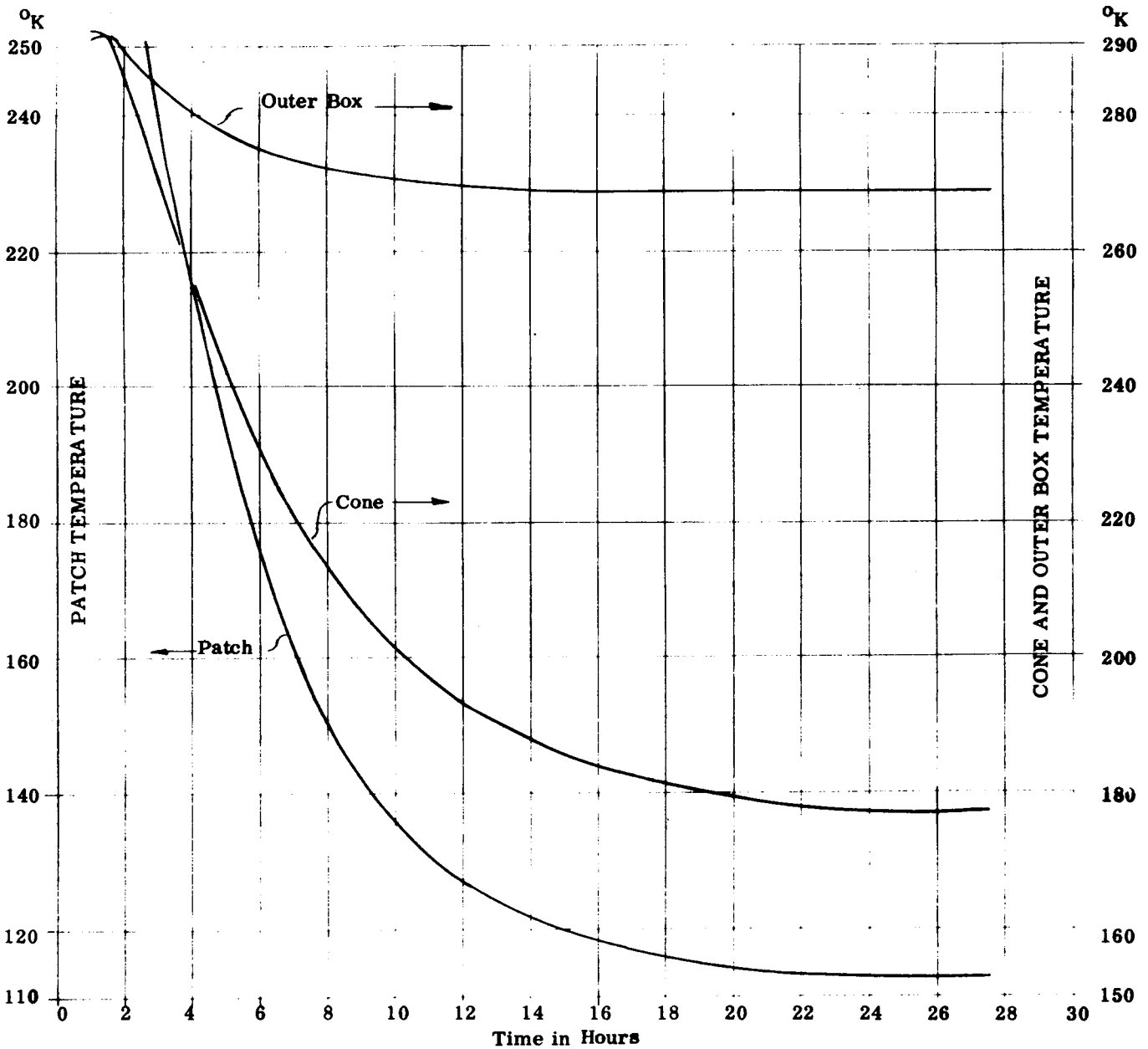

Figure 4 Radiant Cooler Test No. 2 (Au on Al on Alzak Cone)

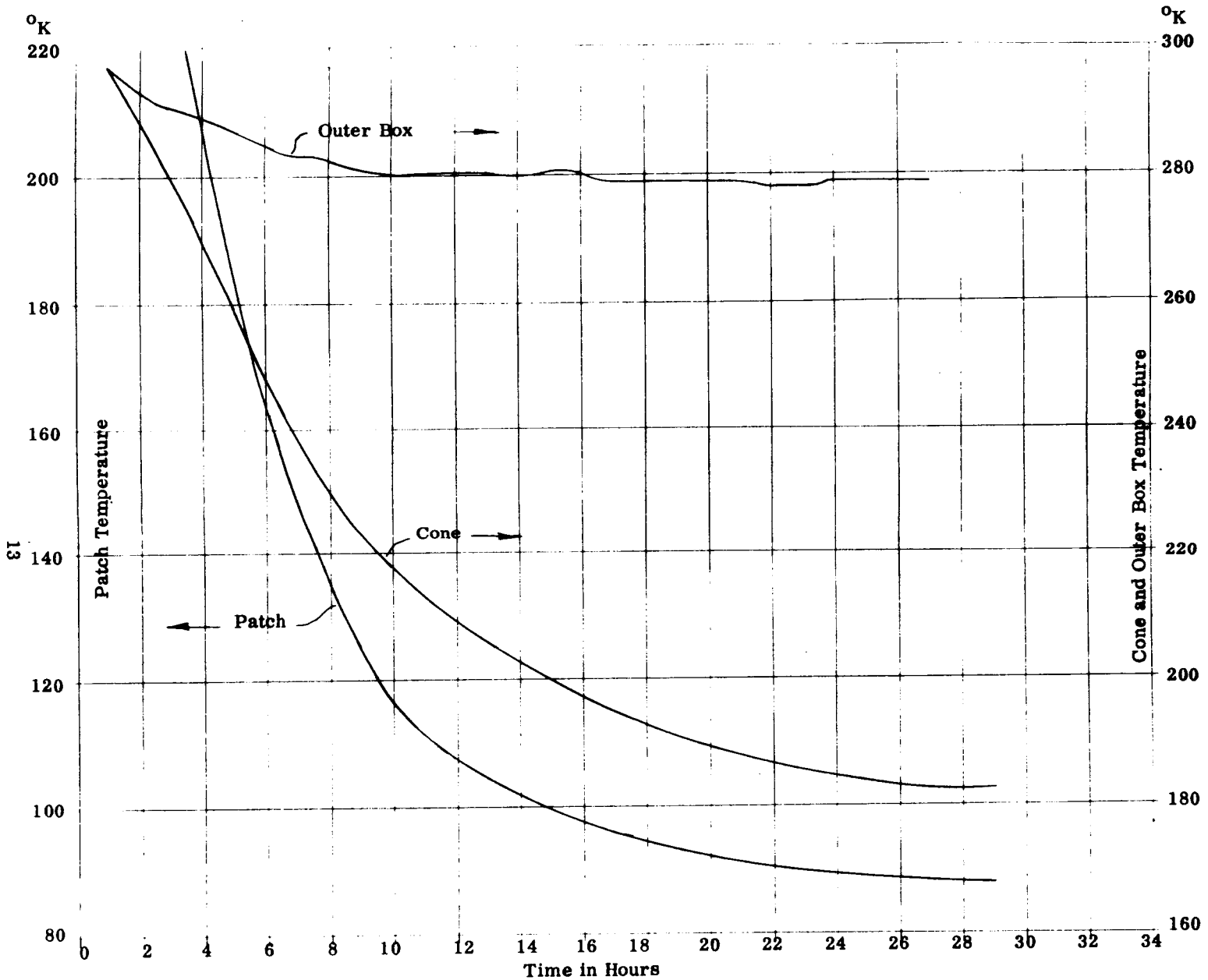

Figure 5 Radiant Cooler Test No. 3 (Aluminized Mylar Cone)

The first sum uses the values of f_n in the vertical plane and the second sum, in the horizontal plane. The value of ϵ_{pc} in a single-stage cooler is given by (First Quarterly Report, Section 5.4)

$$\epsilon_{pc} = \left(\frac{T_p}{T_c}\right)^4 \tag{2}$$

where T_p = patch temperature

T_c = cone temperature

The values of f_n are given in Table 2, p. 24, of the First Quarterly Report. Substituting them into equation (1), we obtain

$$\epsilon_g = 1 + \frac{1.075 - [(1.075)^2 + 1.276\,(1.394 - 2\,\epsilon_{pc})]^{1/2}}{0.638} \tag{3}$$

The values of ϵ_g were calculated for the two models of radiant cooler described in Section 4.1. The results are given in Table 1.

Table 1

Experimental Values of Cone Surface Emissivity

Cone Wall Material	T_p/T_c	ϵ_{pc}	ϵ_g
Au on Aℓ on Alzak	0.638	0.166	0.202
Aℓ on Mylar	0.481	0.0535	0.063

The value of box-cone emissivity for a single-stage cooler in the space chamber can be determined from the thermal balance equation of the cone (Second Quarterly Report, Section 5.5.1)

$$A_{ce}\ \sigma\ T_c^4 + A_c\ \sigma\ T_c^4\ (\epsilon_{cx} + \epsilon_{cp}) = A_c\ \epsilon_{bc}\ \sigma\ (T_s^4 - T_c^4) \tag{4}$$

where T_s = temperature of outer box

A_{ce} = area of cone ends

A_c = area of cone walls

ϵ_{cx} = effective external emissivity of the cone

ϵ_{cp} = effective cone-to-patch emissivity

Solving for ϵ_{bc}, we obtain

$$\epsilon_{bc} = \frac{\frac{A_{ce}}{A_c} + \epsilon_{cx} + \epsilon_{cp}}{\left(\frac{T_s}{T_c}\right)^4 - 1} \tag{5}$$

The value of A_{ce}/A_c is 0.118. Equation (4) assumes close-spaced or plane-parallel geometry, so there is no distinction between box-to-cone and cone-to-box emissivity.

The effective cone-to-patch emissivity is related to the effective patch-to-cone emissivity by (First Quarterly Report, equation 15)

$$\epsilon_{cp} = \frac{A_p}{A_c} \cdot \epsilon_{pc} \tag{6}$$

where A_p is the radiating area of the patch The value of A_p/A_c is 0.065. The effective cone external emissivity is given by (First Quarterly Report, p. 26)

$$\epsilon_{cx} = \frac{A_m}{A_c} \left[1 - \sum_{n=0} f_n' (1 - \epsilon_g)^n\right] \tag{7}$$

where A_m = area of cone mouths

f_n' = view factor from cone mouth to cone mouth and patch as seen by n reflections in the cone walls

The values of f_n' are listed in Table 3, p. 26, of the First Quarterly Report. The value of A_m/A_c is 0.316.

Values of ϵ_{cp}, ϵ_{cx}, and ϵ_{bc} were calculated for the two cooler models. The results are listed in Table 2.

Table 2

Experimental Values of Effective Emissivities

Cone Wall Material	ϵ_{cx}	ϵ_{cp}	ϵ_{bc}
Au on Aℓ on Alzak	0.105	0.0109	0.054
Aℓ on Mylar	0.0375	0.00348	0.036

In both cooler models the inner surface of the outer box (i.e., the surface facing the cone) was lined with aluminized mylar. In the first cooler the outer surface of the cone was anodized aluminum and in the second, clean mill-finished aluminum. The lower emissivity of the second cone surface produced a lower value of box-cone emissivity.

4.3 Thermal Simulation

If the temperature of the first-stage cone approximates its in-orbit value during thermal space chamber tests, the patch temperatures will also be close to their orbital values and the test will be realistic. The in-orbit cone temperature for a cone surface of aluminized mylar is calculated below for an orbit normal to sun angle of 79 degrees. The cone temperature during the third thermal test was about 10 percent below this temperature, so that the patch temperature was also 10 percent below its orbital value. Closer simulation can be obtained by increasing the radiative coupling from the outer box to the first-stage cone, thereby increasing the cone thermal load and cone temperatures.

The in-orbit temperature of the first-stage cone is calculated in Section 5.1 of the Second Quarterly Report at the extreme values of cone surface emissivity (ϵ_g) and solar absorptivity (α_g). The same procedure may be used to calculate the in-orbit cone temperature for an aluminized mylar surface. If we assume α_g equals 0.20[1] (L. H. Hemmerdinger and R. J. Hembach in "Handbook of Military Infrared", Ed. by W. Wolfe, Office of Naval Research, 1965, p. 804) and ϵ_g equals 0.063 (Section 4.2), the in-orbit cone temperature is

$$T_c = 203^{\circ}K \tag{8}$$

for an orbit normal to sun angle of 79 degrees and an earth shield attached to the outer box (First Quarterly Report, Section 4.3). The values of the other parameters are given in Section 5.1 of the Second Quarterly Report, except those depending on ϵ_g and α_g which have the following values

$$\epsilon_{cx} = 3.75 \times 10^{-2}$$

$$\epsilon_{cp} = 3.48 \times 10^{-3}$$

$$\epsilon_{ce}^{s} = 6.64 \times 10^{-3}$$

$$\alpha_{ce}^{s} = 1.80 \times 10^{-2}$$

$$H = 5.75 \times 10^{-4} \text{ watts/cm}^2$$

From equation (2) and Table 1, the corresponding in-orbit patch temperature is

$$T_p = 97.5^{\circ}K \tag{9}$$

---

1 On the other hand, W. B. Fusscell, et. al., in "Measurement of Thermal Radiation Properties of Solids", Ed. by J. C. Richmond, NASA SP-31, 1963 give $\alpha_g = 0.13$ for aluminized mylar (p. 100).

If the 1-1/16-inch wide cone ends in a flight model are made of Alzak treated aluminum, better values for the emissivity and solar absorptivity of the ends are (Hemmerdinger and Hembach, op. cit.)

$$\epsilon_d = 0.8$$

$$\alpha_d = 0.15$$

This reduces the absorbed direct solar power per unit cone wall area to

$$H = 5.58 \times 10^{-4} \text{ watts/cm}^2$$

For the other parameters as above (aluminized mylar cone walls), the cone and patch temperatures become

$$T_c = 206^{\circ}K$$

$$T_p = 99^{\circ}K$$

To increase the accuracy of the simulation of in-orbit thermal conditions, the in-chamber cone temperature will be increased in future tests by increasing the box-cone radiative coupling. If the aluminized mylar is removed from the inner surface of the outer box, it exposes three box walls of mill-finished aluminum and one of Alzak treated aluminum (the outer box surface facing the spacecraft is mill-finished aluminum). The resultant in-chamber cone temperature is close to its orbital value, as shown by the following calculations.

The emissivity of the mill-finished aluminum can be estimated from the values of box-cone emissivity, ϵ_{bc}, given in Section 4.2. Assuming plane-parallel or close-spaced geometry, we have

$$\epsilon_{bc} = \frac{1}{\frac{1}{\epsilon_1} + \frac{1}{\epsilon_2} - 1} \tag{11}$$

where ϵ_1 = emissivity of inner surface of box

ϵ_2 = emissivity of outer surface of cone

If we assume the anodized aluminum outer cone surface in the first cooler model is black ($\epsilon_2 = 1$), we obtain the minimum value for the aluminized mylar of $\epsilon_1 = 0.054$ (Table 2). Using this value we can calculate the maximum value for the emissivity of the mill-finished aluminum on the outer cone surface in the second cooler model. The result is $\epsilon_2 = 0.098$.

Upon removal of the aluminized mylar from the inner surface of the box in the second model, 0.845 of the surface area becomes mill-finished aluminum facing mill-finished aluminum and 0.155 mill-finished aluminum facing Alzak. The first combination produces a box-cone emissivity of 0.0515 and the second, 0.096 (Alzak emissivity of 0.8). The average box-cone emissivity is then

$$\epsilon_{bc} = 0.845 \times 0.0515 + 0.155 \times 0.096 \qquad (12)$$

$$\epsilon_{bc} = 0.058$$

Using equation (5) and experimental data for the second cooler model (aluminized mylar cone surface), we obtain an outer box to first-stage cone temperature ratio of

$$\frac{T_s}{T_c} = 1.39$$

for $\epsilon_{cb} = 0.058$. For an outer box temperature 279 degrees K (achieved in the third thermal test), the in-chamber cone temperature is

$$T_c = 201^{o}K \qquad (13)$$

This is very close to the estimated in-orbit range of 203 degrees K to 206 degrees K.

4.4 Copper Space Reference

The copper structure used to simulate cold space operated close to its design values. The copper reached thermal equilibrium in about 10.7 hours.[2] The maximum temperature on a copper end plate at thermal equilibrium was about 29 degrees K (measured near the farthest point from the second cold exchanger of the helium refrigerator). The cool-down time is a little longer than the calculated value (9.9 hours, Appendix II). The maximum temperature is about that originally calculated (29 to 30 degrees K, Appendix XII to the First Quarterly Report). The thermal load on the copper structure is determined below using the experimentally measured temperature drop across the copper. The result (38 watts) compares well with the value calculated from equilibrium radiative loading from the chamber and the radiant cooler when the cooler is placed between the two copper end plates (Appendix I). The thermal loads from the aluminum shroud (Third Quarterly Report, Appendix II) and through the support cables to the chamber (Third Quarterly Report, Appendix III) are negligible by comparison. The aluminum shroud was operated without an outer cover of aluminized mylar and attained a thermal equilibrium temperature of about 100 degrees K near the farthest point from the intermediate heat exchanger. Photographs of the copper reference and aluminum shroud suspended inside the chamber are contained in Section 3.0 of the Fourth Quarterly Report.

---

2 Results are given for the first test of the space reference.

The copper space reference contains five parts and five contact areas between parts (the last between a copper piece and the second cold exchanger). From the top of an end plate to the second cold exchanger the total temperature drop across the parts and contacts is given by (See Appendix XII to the First Quarterly Report)

$$\Delta\theta = \frac{1}{2} Q \left[\frac{1}{K}\left(\frac{L_1}{2A_1} + \frac{L_2}{2A_2} + \frac{2L_4}{A_4} + \frac{2L_5}{A_5} + \frac{L_3}{A_3}\right)\right.$$

$$\left. + \frac{1}{h_{c1}}\left(\frac{1}{A_{c1}} + \frac{2}{A_{c3}} + \frac{2}{A_{c4}} + \frac{2}{A_{c5}}\right) + \frac{1}{h_{c2} A_{c2}}\right] \qquad (14)$$

where Q = thermal load, assumed uniformly incident on the end plates (part 1) with half on each end plate

K = thermal conductivity of OFHC[3] copper

L_i = length of conductive path in part i

A_i = cross-sectional area of part i through which heat flows

h_{ci} = heat transfer coefficient between two parts

A_{ci} = contact area between part i and part i + 1

Contacts 1, 3, 4, and 5 are through a silicone grease-silver powder mixture, for which $(h_{c1})^{-1} = 0.3$ cm^2 ^oK/watt (based on experimental data). Contact 2 is between bare parts, for which $(h_{c2})^{-1} = 1.5$ cm^2 ^oK/watt.

The final dimensions of the parts to the copper space reference are given in Table 3. Substituting the data from Table 3 into equation (14), we obtain

$$\Delta\theta = 1/2\ Q \times 0.543\ ^oK,\ Q \text{ in watts} \qquad (15)$$

for K = 12 watts/cm ^oK. The temperature drop, $\Delta\theta$, across the copper structure from the top of an end plate to the second cold exchanger was 10.3 degrees K at thermal equilibrium.

---

3 Trademark of American Metal Climax, Inc.

Table 3

Dimensions of Parts in Space Reference

	Part	L (inch)	A (inch^2)	A_c (inch^2)
1.	End plate	10.5	3.0	21
2.	Bar at bottom of plate	24	3.5	7.45
3.	Half of bar between plates	12	4.33	9.4
4.	Bar from 3 to 5	10	5.0	5.0
5.	Connection to cold exchanger	6.4	5.0	18.1

The thermal load on the copper was then

$$Q = 38 \text{ watts} \tag{16}$$

This is within 10 percent of the estimated load with the radiant cooler in place after the cooler parts have reached thermal equilibrium (42 watts, Appendix I).

4.5 Effect of Non-Black Space Reference

The fact that the space reference is not absolutely black (i.e., does not have zero reflectivity) reduces the net radiation emitted by the patch and increases the radiation absorbed by the patch. Part of the patch and cone radiation reaching the reference is reflected back to the patch. This increases the patch temperature above the level attained with a black reference such as outer space.

The value of the reflectivity for the 3M Black Velvet coating on the space reference is not known. The reference is at about 30 degrees K and the incoming radiation from sources in the temperature range of 80 to 200 degrees K. D. L. Stierwalt (Applied Optics 5, 1914, 1966) shows that the emissivity (absorptivity) of 3M Black Velvet at 77 degrees K is about 0.95 over the wavelength range from 5 to 40 microns. Hemmerdinger and Hembach (chapter 20 in "Handbook of Military Infrared Technology", Ed. by W. L. Wolfe, Office of Naval Research, 1965) list an emissivity value for 3M Black Velvet over zinc chromate primer of 0.92 at 228 degrees K on an alodined aluminum substrate. Scott ("Cryogenic Engineering", D. Van Nostrand, 1959, p. 348) lists an emissivity of 0.97 for black matte lacquer at 373 degrees K. We have therefore selected three values of absorptivity for the space reference, 92, 95, and 98 percent; they correspond to reflectivities of 8, 5, and 2 percent.

A blackbody or graybody source at 200 degrees K has only about 14 percent of its energy at wavelengths above 40 microns. However, at 80 degrees K the percentage is 68. On the other hand, most of the increase in patch temperature is produced by the cone radiation at about 200 degrees K that is reflected off the space reference and absorbed in the patch. From the spectral data of Stierwalt, we may therefore conclude that center value of 5 percent reflectivity probably most nearly represents the actual case. (See also A. R. Karoli, et. al., Applied Optics 6, 1184, July 1967.) It is shown below that a 5 percent diffuse reflectivity increases the patch temperature by about 4.2 percent in the first-stage of a cooler whose cone walls have an emissivity of 0.063.

The fraction of patch radiation returned to the patch by reflection off the space reference is

$$F_{pp} = \rho_{pc}\,\rho_r\,(g_1 + g_2\,\rho_r\,g_1 + g_2^2\,\rho_r^2\,g_1 + \cdots)$$

where ρ_{pc} = fraction of radiant flux from patch that reaches cold reference by reflection in cone (First Quarterly Report, Appendix II)

ρ_r = diffuse reflectivity of cold reference

g_1 = fraction of diffuse radiation from reference that reaches patch by reflection in cone

g_2 = fraction of diffuse radiation from reference that returns to reference by reflection in cone

This is a geometric progression and may be summed to yield

$$F_{pp} = \frac{\rho_{pc}\,\rho_r\,g_1}{1 - g_2\,\rho_r} \tag{17}$$

Similarly, the fraction of cone radiation which reaches the patch by reflection off the diffuse space reference is

$$\epsilon_{cx}\,(\rho_r\,g_1 + \rho_r^2\,g_2\,g_1 + \rho_r^3\,g_2^2\,g_1 + \cdots)$$

where ϵ_{cx} is the effective cone external emissivity (First Quarterly Report, Appendix VIII). Summing this progression and adding it to the fraction that goes directly from the cone to the patch, ϵ_{cp} (First Quarterly Report, Section 4.2.2), we obtain the total fraction of cone radiation absorbed in a black patch

$$F_{cp} = \epsilon_{cp} + \frac{\epsilon_{cx}\,\rho_r\,g_1}{1 - g_2\,\rho_r} \tag{18}$$

The net power emitted by the black patch at a temperature T_p is $(1 - F_{pp}) \cdot \sigma T_p^4 A_p$, where A_p is the area of the patch. The power absorbed from the cone at a temperature T_c is $F_{cp} \sigma T_c^4 A_c$, where A_c is the surface area of the cone walls. Equating these two powers, we obtain the thermal balance equation for the patch and the equation

$$\left(\frac{T_p}{T_c}\right)^4 = \frac{F_{cp}}{\frac{A_p}{A_c}(1 - F_{pp})} \tag{19}$$

In the derivation of the equation for the effective cone external emissivity (First Quarterly Report, pp. 26-27 and Appendix VIII), we obtained the values of f_n', the fraction of diffuse radiation entering the mouth of a perfectly reflecting cone that requires n cone wall reflections to return to the mouth or to go to the patch. The fraction f_n' may be divided into two parts

$$f_n' = f_{np}' + f_{nm}'$$

where f_{np}' = fraction going to patch

f_{nm}' = fraction returning to mouth

The fraction of diffuse radiation from the space reference reaching the black patch by reflection in the cone (but without reflection off the reference) is then

$$g_1 = \Sigma f_{np}' \rho_g^n \tag{21}$$

for a cone surface of reflectivity ρ_g. And the fraction returning to the space reference (cone mouth) by reflection in the cone (but without reflection off the reference) is

$$g_2 = \Sigma f_{nm}' \rho_g^n$$

Values of f_{np}' and f_{nm}' are given in Table 4 for diffuse reflection from the center of the cone mouth in the vertical and horizontal planes of the first-stage. In the vertical plane, about 10 percent of the diffuse emission entering the mouth of a perfect cone goes to the patch and 90 percent goes back out the mouth. In the horizontal plane, about 50 percent goes to the patch and 50 percent back to the mouth.

Table 4

Distribution of Radiation Entering Mouth of Perfect Cone

n	Vertical Plane f'_{np}	Vertical Plane f'_{nm}	Horizontal Plane f'_{np}	Horizontal Plane f'_{nm}
0	0.0116	0	0.306	0
1	0.0587	0.101	0.182	0.166
2	0.0319	0.187	0	0.308
3	0	0.238	0	0.038
4	0	0.229		
5	0	0.1428		
	0.1022	0.8978	0.488	0.512

For a cone wall emissivity (ϵ_g) of 0.063, ρ_g equals 0.937. Using the average of the horizontal and vertical plane values from equations (21) and (22) and the data of Table 4, we then obtain

$$g_1 = 0.2856$$
$$g_2 = 0.5958 \qquad (23)$$

The remaining fraction of reflected radiation, $1 - (g_1 + g_2) = 0.1186$, is absorbed in the cone walls and therefore equals the absorptivity of the conical cavity (First Quarterly Report, Appendix VIII). Multiplying 0.1186 by the ratio of cone mouth to cone wall area, we obtain the effective cone external emissivity of 0.0375 (Equation 7 and Table 2). The values of ϵ_{cp} and ϵ_{cx} for ϵ_g equal to 0.063 are also given Table 2.

The values of F_{pp} anf F_{cp} were calculated according to equations (17) and (18) for reference reflectivities of 0.08, 0.05, and 0.02 The results are listed in Table 5.

Table 5

Fraction of Radiation Reaching Patch
$\rho_g = 0.937$

ρ_r	From Patch F_{pp}	From Cone F_{cp}
0.08	0.02271	0.00438
0.05	0.01393	0.00403
0.02	0.00547	0.00370
0	0	0.00348

The ratio of patch temperature to cone temperature was then determined by equation (19). The results are given in Table 6 for A_p/A_c equal to 0.065.

Table 6

Ratio of Patch to Cone Temperature
$\rho_g = 0.937$

ρ_r	T_p/T_c
0.08	0.5124
0.05	0.50075
0.02	0.4891
0	0.4809

We divided the temperature ratio for a non-zero reference reflectivity by the ratio for zero reflectivity and subtracted unity from the result to obtain the fractional increase in patch temperature produced by a non-black reference. The results are shown in Table 7 as percentage increases.

Table 7

Increase in Patch Temperature Produced by Non-Black Space Reference
$\rho_g = 0.937$

ρ_r	% Increase
0.08	6.6
0.05	4.2
0.02	1.7

4.6 Gas Conduction

The residual gas pressure in the space chamber should be no greater than about 2×10^{-6} Torr if gas conduction is to contribute no more than 1 percent of the thermal load to a patch (Second Quarterly Report, Section 5. 5. 2) When the cooler model with the Alzak cone surfaces was first placed in the chamber, it could not be evacuated because of extensive outgassing. The outgassing was traced to uncured adhesive used to bond the urethane foam core to the aluminum and Alzak skins. The adhesive (Dow Corning Silastic 140) cures by reaction with atmospheric moisture. The cooler model was therefore placed in another vacuum chamber of greater pumping speed to remove a large part of the gas evolved from uncured adhesive. The cooler model with the aluminized mylar surface was constructed of laminated panel purchased from Met-L-Wood Corp. (Chicago, Ill.). This laminate uses an epoxy adhesive which does not depend on air for curing and which does not outgas. In addition, to promote the escape of adhesive gas and the evacuation of air from the foam, small holes were drilled through the outside skin of the cone structure and inside skin of the outer box.

When the Alzak cone model was evacuated in preparation for the first thermal test, the pressure reached only about 4×10^{-4} Torr. After the helium refrigerator was turned on, the copper cold target and aluminum shroud acted as cryopumps and reduced the pressure to a final value of 3.2×10^{-5} Torr. This is still an order of magnitude above the desired level.

The failure to attain a sufficiently low pressure during the first thermal test was apparently due to leaks in the space chamber. These leaks were fixed before starting the second thermal test. The pressure after evacuation of the same Alzak cone model but prior to starting the helium refrigerator for the second thermal test was 2.1×10^{-5} Torr. The cryopumping of the space simulator reduced this to a final value of 2.7×10^{-7} Torr. The final pressure during the third thermal test was 3.7×10^{-7} Torr. The contribution of gas conduction to the thermal loads on the members of the radiant cooler is entirely negligible at these pressures.

5.0 OPTICAL DESIGN

The relay optics transfers radiant energy from the primary focus at the chopper to the secondary focus at the detector element; its specification is given in Appendix III. The first element of the relay optics (used to collimate the radiation from the primary image) will be a doublet lens instead of a paraboloidal mirror and folding flat (First Quarterly Report, Section 4.6; Second Quarterly Report, Section 6.2). The beam from the doublet is focused by an f/8 germanium lens and then increased in speed to f/2 by an aplanatic germanium lens that focuses radiation on the detector element. The design of the f/8 lens is outlined below; the design of the aplanatic lens is described in Section 5.1 of the Fourth Quarterly Report. The two elements and their spacing are shown in Figure 6.

A lens bent for minimum spherical aberration has a nearly flat second surface when its refractive index is high (R. M. Scott, "Optics for Infrared Systems", Proc. IRE 47, 1530, Sept. 1959). We will therefore consider such a design for the f/8 germanium lens. The Coddington shape factor is then

$$\sigma = \frac{r_2 + r_1}{r_2 - r_1} = 1 \qquad (24)$$

where r_1 = radius of lens surface nearer object

r_2 = radius of lens surface nearer image

The paraxial focal length of the lens for a flat second surface ($r_2 = \infty$) is independent of the lens thickness and given by

$$f' = \frac{r_1}{n-1} \qquad (25)$$

where n is the refractive index. For r_1 = 10.0 inches and n = 4 (Ge at 11 microns)

$$r_1 = 30.0 \text{ inches} \qquad (26)$$

The diameter of the primary spherical aberration at best focus for an object at infinity is given by

$$\delta_{SA} = \frac{f'}{64N^3} A \qquad (27)$$

where N is the f-number of the focused beam and A is given by

$$A = \frac{n+1}{n(n-1)^2} \sigma 2 - \frac{4(n+1)}{n(n-1)} \sigma + \frac{3n+2}{n} + \frac{n^2}{(n-1)^2} \qquad (28)$$

For σ = 1 and n = 4

$$A = 34/9 \qquad (29)$$

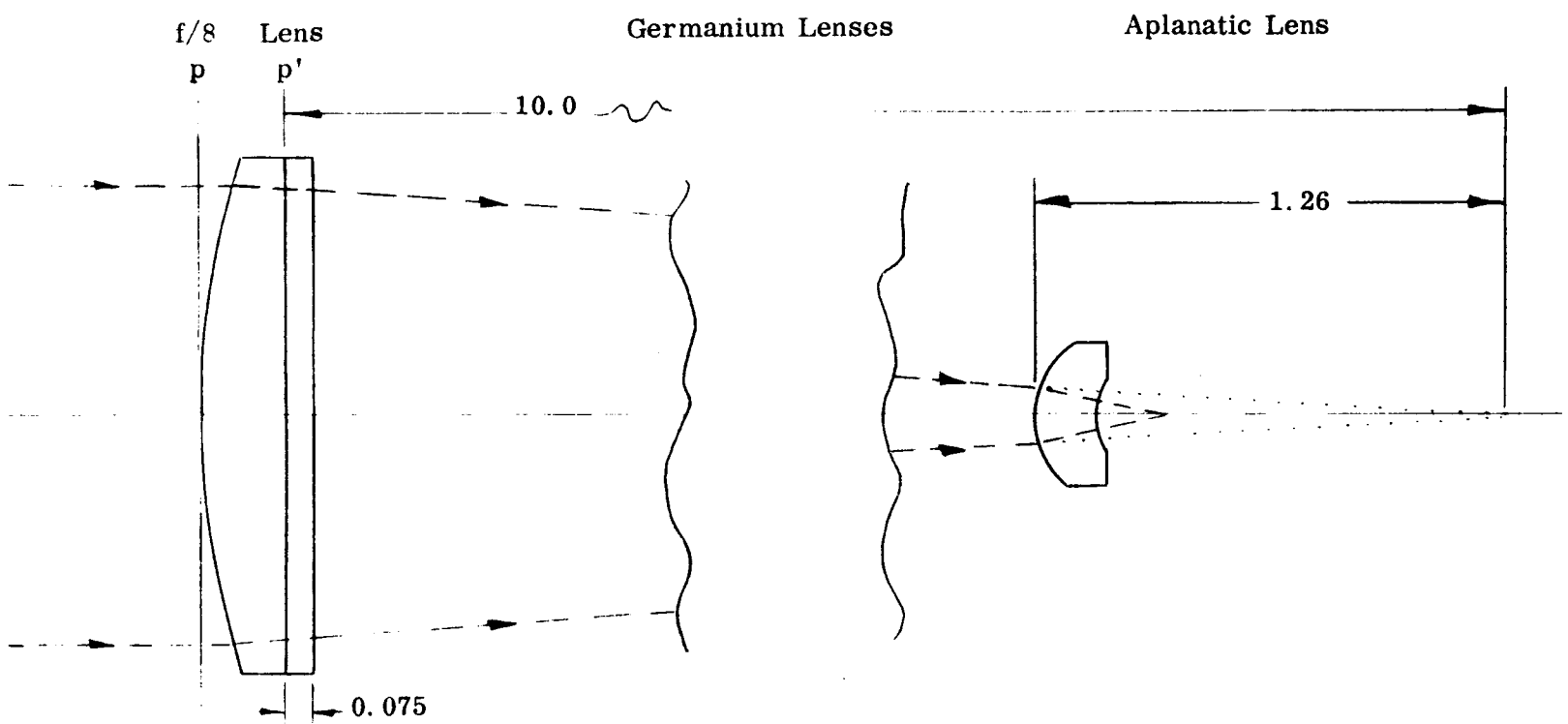

Figure 6 Relay Optic Design Following Collimation

Then for f' = 10.0 inches and N = 8

$$\delta_{SA} = 1.15 \times 10^{-3} \text{ inch} \tag{30}$$

The corresponding value for the longitudinal spherical aberration, or paraxial focal length minus marginal focal length, is

$$(LA)' = \frac{f'}{32N^2} A = 18.40 \times 10^{-3} \text{ inch} \tag{31}$$

Because of the small field of view (2.5×10^{-3} radian square at the primary image) the only off-axis aberration of any consequence is coma. For the exit pupil at a thin lens, the comatic radius is given by (F. A. Jenkins and H. E. White, "Fundamentals of Optics", McGraw-Hill, 1950, p. 134)

$$r_c = \frac{y}{4f'N^2} (G\rho + W\sigma) \tag{32}$$

where y = off-axis distance of image point

$\rho = \frac{s' - s}{s' + s}$ = Coddington position factor[4]

s' = image distance

s = object distance

$G = \frac{3(2n + 1)}{4n}$

$W = \frac{3(n + 1)}{4n (n - 1)}$

For an object at infinity ($\rho = -1$)[5] and for germanium (n = 4)

$$r_c = -\frac{11y}{32N^2} \tag{33}$$

At the corner of the field of view, y = 0.055 inch; then, for N = 8

$$r_c = -0.30 \times 10^{-3} \text{ inch} \tag{34}$$

---

4 Sign convention of Jenkins and White

5 Also equal to -1 for sign convention of Conrady

Because the exit pupil is not located at the lens (See Second Quarterly Report, Figure 13), the above value of coma must be corrected for a shift in the pupil from the lens to its actual position. For coma measured by its radius (sagittal coma) the change produced by a pupil shift is given by (A. E. Conrady, "Applied Optics and Optical Design", Dover 1957, pp. 336, 341-343)

$$\Delta r_c = \frac{(LA)' W' y}{2Nh} \tag{35}$$

where[6]

$$W' = \frac{\ell'^*_{pr}}{\ell' - \ell'^*_{pr}} \tag{36}$$

ℓ' = image distance = f' = 10.0 inches

ℓ'^*_{pr} = distance from lens to final position of exit pupil

h = radius of effective lens aperture = 0.625 inch

From the Second Quarterly Report, Figure 13

$$\ell'^*_{pr} = -9.46 \text{ inches} \tag{37}$$

Then for y = 0.055 inch, N = 8, and the above value of longitudinal spherical aberration

$$\Delta r_c = +0.05 \times 10^{-3} \text{ inch} \tag{38}$$

The comatic radius for the actual position of the aperture is then

$$r_c^* = -0.25 \times 10^{-3} \text{ inch} \tag{39}$$

The maximum allowable diameter at the image plane of the f/8 lens is 4×10^{-3} inch (Third Quarterly Report, Table 8, p. 25). The design of the f/8 lens therefore meets all the requirements. The lens is shown in Figure 6 in relation to the aplanatic lens; the positions of its principal planes are also given.

---

6 The formula for W' is for the exit pupil initially at the lens.

6.0 VIDEO ELECTRONICS

Figure 7 is a schematic of the video electronics shown with certain test equipment and test circuitry. Most circuits, it can be seen, utilize a microcircuit monolithic amplifier, the μa 709. This circuit component can be used for a-c or d-c amplification, as a comparator, and as a multivibrator. The signal fed to the video amplifier from the microvolter will eventually come from the preamplifier. The attenuated signal shown going to the reference signal generator simulates the photodiode signal induced by the chopped light through the mechanical chopper.

6.1 Reference Voltage Generator

The reference voltage generator, comprised of Amp 3, Amp 4 and other components, processes 6 khz signal from the chopper photodiode to a 6 khz square wave for demodulation of the video signal. Amp 3 is an a-c amplifier with a voltage gain variation of 5.6 db. Amp 4 is a saturating amplifier which squares up the video signal until now, a sinusoidal signal. The output is a 6 khz square wave approximately 22 volts peak to peak.

6.2 Video Amplifier

This circuit serves as an amplifier and as a driver for the demodulator. The maximum amplifier gain is about 60 db with a variation of 6 db. The low frequency cutoff is about 700 hz, and the high frequency cutoff, 47 khz at maximum gain, is 70 khz at minimum gain.

6.3 Demodulator and Low-Pass Filter

The circuitry consisting of T_1, T_2, Q_1, Q_2, CR1, CR2, R5, R6, R7, R8, R9, R11, R12, C5 and C29 is the demodulator. This circuit synchronously rectifies the video amplifier output. The switching voltage from the reference signal generator is fed in at T_2. The rectified output is applied at the common source connection of the CM602's Q_1 and Q_2.

The low-pass filter is made up of L_1, L_2, C_6, C_7 and R_{10}. The filter response with the demodulator is shown in Figure 8. The filter causes a delay which is constant for all frequencies over the pass band. This delay was found to be 184 microseconds.

6.4 Output Amplifier

The output amplifier (Amp 2, etc.) provides amplification of the demodulated and filtered signal from d-c to beyond the pass band. It also serves as a mixing point for the video and chopper correction input.

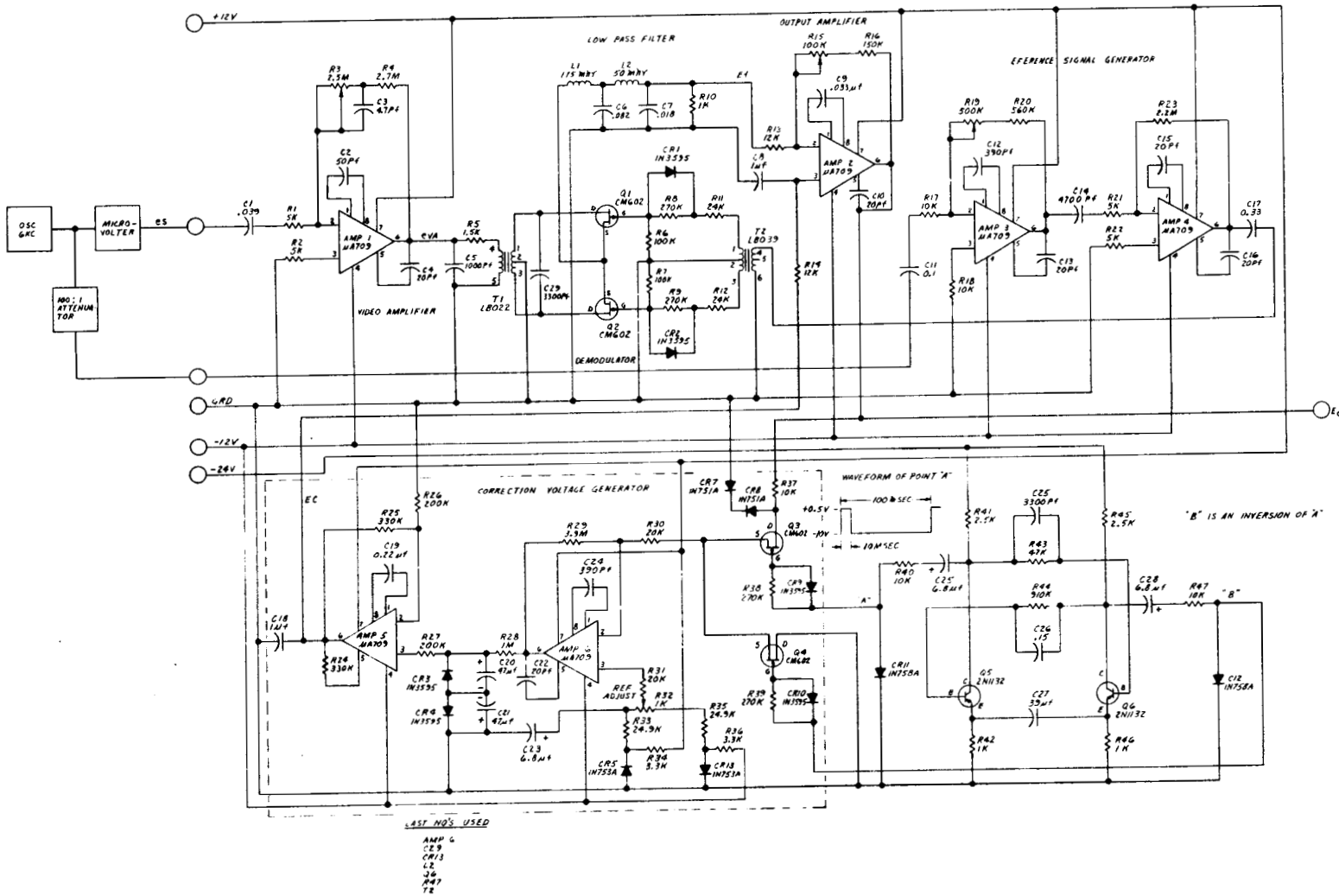

Figure 7 Schematic, Two Stage Cooler Video Loop Testing Configuration

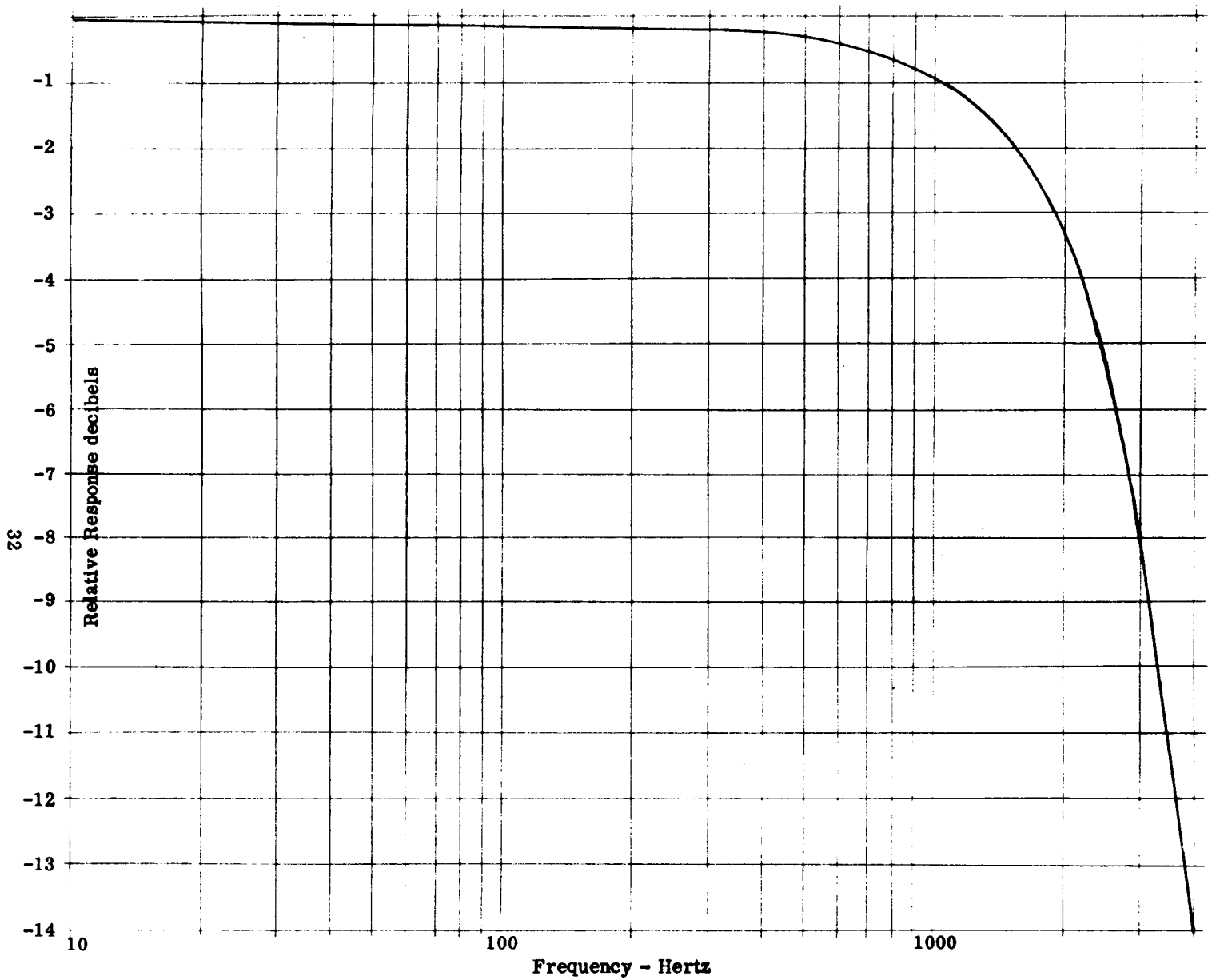

Figure 8 Demodulator and Low Pass Filter Response

6.5 Correction Voltage Generator

Shown within the dotted lines on Figure 7, the correction voltage generator provides output correction for the difference in signal between the chopper and space. The gate formed by Q_3, etc. passes the video output to the comparator (Amp 6, etc.) during the time that the mirror is scanning space. This time period is assumed to be one-tenth of the total scanning time. For the purposes of testing, a space scan monostable multivibrator is simulated by the circuit including Q_5 and Q_6. During the other 90 msec of the scan, Q_4 gates the comparator input to ground. (This simulates a scanning rotation of about 600 rpm as compared to the 100 rpm to be expected. However, the ratio of sampling time to scanning time will remain the same for any speed and thus the over-all gain is not affected).

If the output signal (E_o) is positive with respect to the reference, the comparator has a negative going output and the opposite is true for a negative going input. If the comparator input is equal to the reference level, the comparator output is zero. This pulsed output with a one-tenth duty cycle is integrated by R28 and C20 and C21. (Capacitors C20 and C21 together with diodes CR3 and CR4 make a single bipolar 47 microfarad capacitor). The integrated d-c level is amplified by the non-inverting amplifier Amp 5 which provides the correcting input to the output amplifier through R14.

The correction voltage generator has a gain characteristic such that $E_o = m \cdot E_c + v_{th}$ where E_o is the input voltage level. If the reference level is perfectly adjusted, v_{th} is zero. In measurements taken in the laboratory m had a value of 1/26.8 and v_{th} was +0.025 volts.

6.6 Chopper Correction Loop Calculations

Referring again to Figure 7, it can be seen that the significant part of the above loop with respect to the chopper error is the output amplifier and the correction voltage generator. The following definitions are made:

E_f = the demodulated and filtered video signal input to the output amplifier

E_c = the chopper correction d-c input to the output amplifier

E_o = the video amplifier output and the input to the correction voltage generator

E_{ch} = that portion of the demodulated video signal caused by the chopper

E_{tar} = that portion of the demodulated video signal caused by the target

We then have $E_f = E_{ch} - E_{tar}$, $E_o = K_1 E_F + K_2 E_c$, and $E_c = K_3 (E_o + vth)$. Then $E_o = K_1 (E_{ch} - E_{tar}) + K_2 E_c$. If $E_{tar} = 0$, (which is the case when looking at space), then $E_o (E_{tar} = 0) = K_1 E_{ch} + K_2 E_c$. Therefore $E_c = K_3 (K_1 E_{ch} + K_2 E_c + vth)$ or $E_c = K_1 K_3 E_{ch}/(1 - K_2 K_3) + K_3 vth/(1 - K_2 K_3)$. This is the correction signal caused by a look at space. Working this back into the original equation $E_o = K_1 E_{ch} - K_1 E_{tar} + K_2 E_c$, we have

$$E_o = K_1 E_{ch} - K_1 E_{tar} + \frac{K_1 K_2 K_3 E_{ch}}{(1 - K_2 K_3)} + \frac{K_2 K_3 v_{th}}{(1 - K_2 K_3)}$$

$$E_o = \frac{K_1 E_{ch}}{(1 - K_2 K_3)} - K_1 E_{tar} + \frac{K_2 K_3 v_{th}}{1 - K_2 K_3} \quad (40)$$

From laboratory measurements, $K_1 = -12.8$, $K_2 = 13.7$, $K_3 = 26.8$, $v_{th} = +0.025$; so that

$$E_o \cong 0.035 E_{ch} + 12.8 E_{tar} + v_{th} \quad (41)$$

For a maximum output of 6V, $E_{tar} = 0.47$V for a 330 degree K target. Considering the chopper to have a maximum effective temperature of 300 degrees K, the chopper signal input to the output amplifier is 0.329 V. With $E_{tar} = 0$, $E_o = 0.0115 + 0.025$ and the maximum error at the output due to the chopper correction is 11.5 millivolts.

7.0 NEW TECHNOLOGY

No items which are considered new technology according to the NASA New Technology clause of September 1964 were developed during the fifth quarter of the contract.

8.0 PROGRAM FOR NEXT QUARTER

During the sixth quarter, we plan to conduct thermal-vacuum tests on a complete two-stage radiant cooler and to complete the design of the breadboard radiometer. The test equipment for the radiometer will be installed and tested. Depending on the available time and the inspection and acceptance of Phase II by the Technical Officer, construction of the breadboard radiometer will be started.

9.0 CONCLUSIONS

From vibration and thermal tests conducted during the fifth quarter and an analysis of the thermal test results, we may conclude the following:

a. The two-stage patch assembly (first-stage patch, second-stage cone, and second-stage patch) is vibrationally sound when the first-stage patch is held by a simple 4 pin caging mechanism.

b. Evaporation of a basically low emissivity material such as aluminum or gold on Alzak treated aluminum does not produce a low emissivity surface.

c. Evaporation of aluminum on mylar produces a specular, low emissivity surface suitable for the cone walls in a radiant cooler.

d. Single-stage radiant cooling to 98 degrees K or less can be achieved in a Nimbus orbit at an orbit normal to sun angle in the range 79 to 90 degrees.

e. A space reference at a temperature of about 30 degrees K can be obtained by conductively cooling a large mass of high conductivity copper with a Norelco A-20 helium refrigerator.

f. The conditions for thermal simulation of orbital conditions (proper cone temperature and low residual gas pressure) can be realized.

In general, we are well on our way toward demonstrating the feasibility of two-stage radiant cooling (second-stage temperature below 80 degrees K) under realistic mechanical and thermal conditions.

APPENDIX I

THERMAL LOAD ON COPPER COLD REFERENCE

The thermal load on the copper cold reference used to simulate cold space (First Quarterly Report, Appendix XII) was estimated with and without the radiant cooler in place. In both cases, the back sides of the plates simulating space are shielded from ambient sources by an aluminum shroud connected to the intermediate cold exchanger of the helium refrigerator (Third Quarterly Report, Appendix II). The thermal load from the shroud is negligible compared to that from other sources. The front sides of the copper plates face the cooler and are painted black; they receive most of the thermal loading, as radiation from the space chamber or from the cooler. In addition, portions of the copper connections between the plates and second cold exchanger of the helium refrigerator are unshielded and thermally loaded by ambient radiation.

With the radiant cooler in place, the calculated initial load on the copper reference with the cooler at ambient temperature is about 90 watts. However, this decreases to about 40 watts when the cooler parts have reached their thermal equilibrium temperatures. With a 15 watt load on the intermediate cold exchanger, the second cold exchanger will reach about 15 degrees K at the 40 watt load (Third Quarterly Report, Figure II-2). This is below the nominal design temperature of 17 degrees K (First Quarterly Report, Appendix XII). With the radiant cooler removed from between the black copper plates, the greater input from ambient sources increases the load to about 133 watts. With a 15 watt load on the intermediate cold exchanger, the temperature of the second cold exchanger is increased to about 28 degrees K (Third Quarterly Report, Figure II-2).

The exposed copper area between the plates and the second cold exchanger is loaded by ambient sources whether or not the cooler is in place. The total area exposed to the ambient is about 306 square inches. For the surroundings at 296 degrees K, the ambient thermal load is then

$$\Phi_{con.} = 0.1 \times 2.81 \times 10^{-1} \frac{\text{watts}}{\text{in}^2} \times 306 \text{ in}^2$$

$$\Phi_{con.} = 8.6 \text{ watts} \qquad \text{(I-1)}$$

for a copper emissivity (absorptivity) of 0.1.

Load with Cooler in Place

With the cooler in place, the black sides of the copper plates see ambient or near-ambient sources beyond the edge of the cone, as shown in Figure I-1.

0.5" Dimension Exaggerated to Show Separation

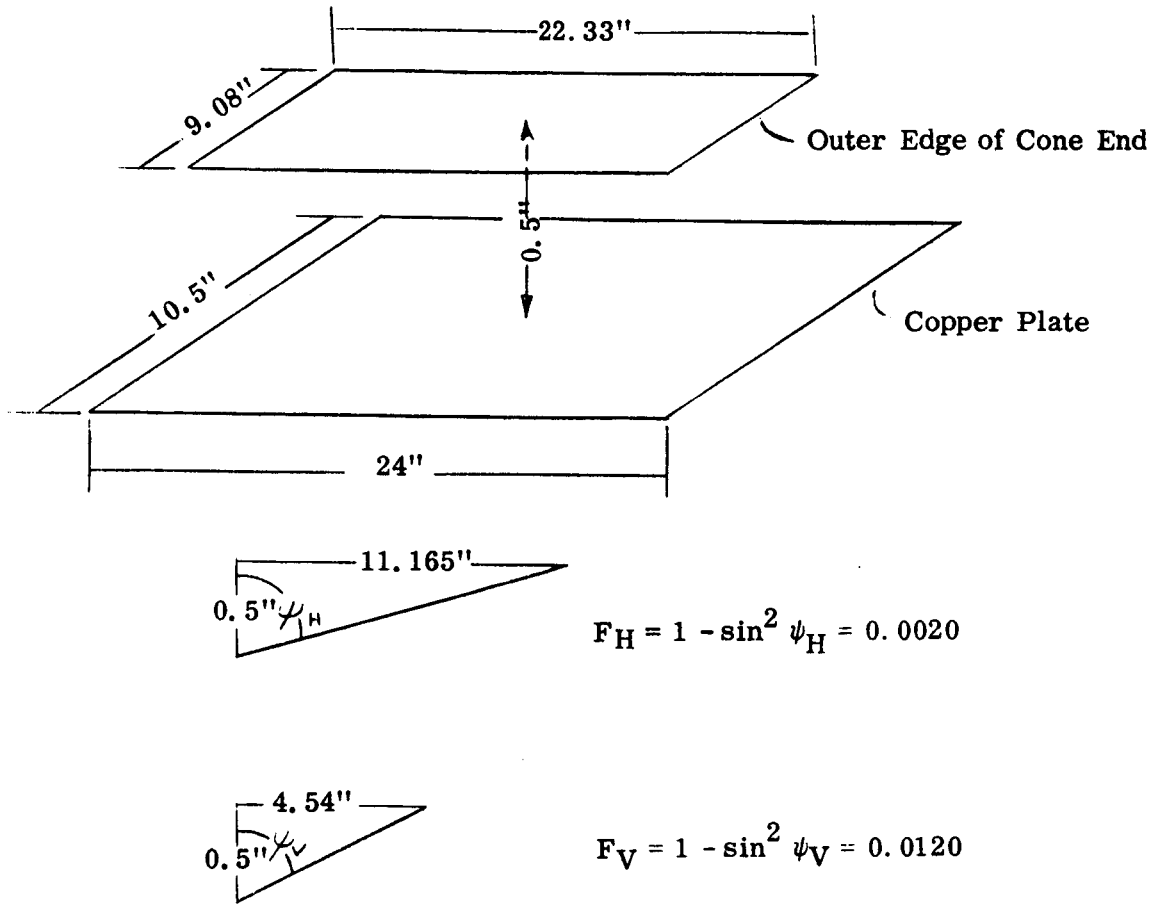

Figure I-1 Plate to Ambient Geometry with Cooler in Place

The cone mouth and cone end are 0.5 inch from the plate. The view factor from the center of the copper plate to the ambient in the horizontal plane is given by

$$F_H = 1 - \sin^2 \psi_H = \frac{0.25}{124.9} = 0.0020$$

And the view factor in the vertical plane is

$$F_V = 1 - \sin^2 \psi V = \frac{0:25}{20.86} = 0.0120$$

The average view factor from the center of a plate to ambient is then 0.007 with the cooler in place, and the ambient thermal load on the plates is about

$$\Phi_a = 2.81 \times 10^{-1} \frac{\text{watts}}{\text{in}^2} \times 512 \text{ in}^2 \times 7 \times 10^{-3}$$

$$\Phi_a = 1.0 \text{ watt} \qquad \text{(I-2)}$$

The two plates are black and have an area of 512 square inches.

To determine the thermal load on the plates with the cooler in place, we need to know the load from the outer box, the first-stage cone (ends and walls), and the patches. The last two loads change as the cooler approaches thermal equilibrium. At first, the entire cooler is at ambient and introduces a larger thermal input to the copper plates.

The outer box is constructed of 3/4-inch laminate, its open ends face the black copper plates and have inner dimensions, in inches, of 9.8 x 22.8. The copper end plates have corresponding dimensions of 24 x 11. Since the foam core is essentially black in the infrared, the loading from both ends of the outer box at ambient (296 degrees K) is

$$\Phi_b = 2 (24 \times 11 - 9.8 \times 22.8) \text{ in}^2 \times 0.281 \text{ watts/in}^2$$

$$\Phi_b = 22.8 \text{ watts} \qquad \text{(I-3)}$$

From equation (9) of the Second Quarterly Report, the outgoing power radiated by the cone walls and cone ends is

$$\Phi_c = A_c \sigma T_c^4 \left[\epsilon_d \frac{A_d}{A_c} + \epsilon_{cx}\right] \qquad \text{(I-4)}$$

The term

$$\epsilon_{cp} \left(1 + 1/2 \frac{A_{c2}}{A_{p1}}\right)$$

represents radiation to the patch and second-stage cone and is not included.

The symbols have the following meanings

A_c = area of cone walls

T_c = temperature of cone

A_d = area of cone ends

$\frac{A_{c2}}{A_{p1}}$ = ratio of outer surface area of second-stage cone to area of first-stage patch

ϵ_d = emissivity of cone end

ϵ_{cx} = effective external emissivity of cone walls

ϵ_{cp} = effective cone-to-patch emissivity

Essentially all the radiation emitted out the cone mouths and by the cone ends is absorbed in the black plates.

For $\epsilon_d = 0.9$ and $A_d/A_c = 0.1356$, equation (I-4) becomes

$$\Phi_c = A_c \sigma T_c^4 \quad [0.122 + \epsilon_{cx}] \qquad \text{(I-5)}$$

The value of the quantity in brackets was evaluated for gold emissivities on the cone walls of 0.086 and 0.02 (First Quarterly Report, Section 4.2.2). The results are shown in Table I-1. The corresponding equilibrium cone temperature and blackbody emittances are listed in Table I-2 together with the blackbody emittance at ambient (296 degrees K).

Table I-1

Emissivity Values

ϵ_g	ϵ_{cx}	$0.122 + \epsilon_{cx}$
0.086	0.05015	0.1722
0.02	0.00940	0.1314

Table I-2

Cone Temperatures

ϵ_g	T_c, ^oK	σT_c^4, watts/in^2
---	296	2.81×10^{-1}
0.086	199	5.735×10^{-2}
0.02	219	8.41×10^{-2}

The cone temperatures at thermal equilibrium are taken from Table 2, p. 29, of the Second Quarterly Report.

Substituting the data in Tables I-1 and I-2 into equation (I-5), we obtain the the thermal loading of the copper plates by the cone. The area, A_c, of the cone walls is 933 square inches (Second Quarterly Report, p. 5). The results are listed in Table I-3.

Table I-3

Loading by First-Stage Cone

ϵ_g	Φ_c with cone at 296^{o}K	Φ_c with cone at thermal equilibrium
0.086	45.1 watts	9.2 watts
0.02	34.5 watts	10.3 watts

The thermal load from the second-stage cone is small compared to that from the patches and the first-stage cone and will be neglected. The thermal load from the black patches is nearly equal to the power emitted by the patches. The emitted power is given in Table I-4 for the patches at thermal equilibrium (Third Quarterly Report, Section 4.3). The two patches have a total radiating area of 72.85 square inches and radiate 20.5 watts at ambient temperature.

Table I-4

Power Radiated by Patches

ϵ_g	First Stage	Second Stage	Total
0.086	0.4 watt	< 0.01 watt	0.4 watt
0.02	0.1 watt	< 0.01 watt	0.1 watt

By adding the thermal loads on the connections and plates, we obtain the total load on the copper reference. The results are shown in Table I-5 for the cooler at ambient and at thermal equilibrium for the two values of gold emissivity.

Table I-5

Thermal Load with Cooler in Place

ϵ_g	Cooler at ambient	Cooler at thermal equilibrium
0.086	98.0 watts	42.0 watts
0.02	87.4 watts	42.8 watts

Load with Cooler Out

With the radiant cooler removed from between the copper plates, each black plate views ambient temperature sources except for the opposite plate (this neglects the small view to the bar connecting the plates). The view factor from one plate to the other is given by (M. Jakob, "Heat Transfer", Vol. II, Wiley and Chapman & Hall, 1957, eq. 31-48)

$$F_{1-2} = \frac{1}{\pi}\left[\frac{1}{BC}\ell n\,\frac{1+B^2+C^2+B^2C^2}{1+B^2+C^2} - \frac{2}{B}\tan^{-1}C + \frac{2}{C}\sqrt{1+C^2}\,\tan^{-1}\frac{B}{\sqrt{1+C^2}} - \frac{2}{C}\tan^{-1}B + \frac{2}{B}\sqrt{1+B^2}\,\tan^{-1}\frac{C}{\sqrt{1+B^2}}\right] \qquad (I\text{-}6)$$

$B = b/a$

$C = c/a$

where each plate has dimensions of b x c and the plates are separated by a distance a. For the copper plates, we have

$a = 21.7$ inches

$b = 24$ inches

$c = 10.5$ inches

Equation (I-5) then yields

$$F_{1-2} = 0.132$$

The view factor from a plate to ambient is

$$1 - F_{1-2} = 0.868$$

and the thermal load on both plates becomes

$$\Phi_a = 512 \text{ in}^2 \times 2.81 \times 10^{-1} \text{ watts/in}^2 \times 0.868$$

$$\Phi_a = 124.9 \text{ watts} \qquad \text{(I-7)}$$

for an ambient temperature of 296 degrees K.

Adding the 8.6 watt load on the copper connections, we obtain the total thermal load, Φ_t, on the copper reference when the radiant cooler is removed.

$$\Phi_t = 133.5 \text{ watts} \qquad \text{(I-8)}$$

APPENDIX II

COOL-DOWN TIME OF COPPER COLD REFERENCE

The time, T, needed to cool the copper reference used to simulate cold space in the vacuum chamber can be estimated by

$$T = \frac{\text{thermal capacity x temperature drop}}{\text{average cold production}}$$

The thermal capacity, C, can be calculated from

$$C = \text{volume x density x specific heat}$$

The copper reference has a volume of about 482 cubic inches including the connections to the second cold exchanger of the helium refrigerator. Copper has a density of 0.321 pounds/in^3 ("Machinery's Handbook", E. Oberg and F. D. Jones, 14th Ed., The Industrial Press, 1953), so the structure weighs about 155 pounds. The specific heat of copper as a function of temperature is shown in the following table ("Handbook of Chem. and Phys.", 44th Ed., Chemical Rubber Pub. Co., 1962, pp. 2352-2353).

Temperature, ^oK	Specific Heat, cals/gm ^oC
20	0.0031
84	0.0506
123	0.0674
173	0.0783
223	0.0862
273	0.0910
293	0.0921

The average specific heat between 293 degrees K and 20 degrees K is 0.067 calories/gram degrees C. The thermal capacity is then

$$C = 155 \text{ lbs} \times 0.067 \text{ cals/gm}^oC \times 1898.64 \text{ gm-joules/lb - cal}$$

$$C = 1.97 \times 10^4 \text{ joules/}^oC$$

The copper is cooled from about 296 degrees K to 16 degrees K, a drop of 280 degrees K. The average cold production at the second cold exchanger is 155 watts between 57 degrees K and 20 degrees K (Third Quarterly Report, Figure II-2). Using this value for cold production, we obtain the following estimate of cool-down time of the copper cold reference

$$T = \frac{1.97 \times 10^4 \times 280}{155 \times 3.6 \times 10^3} \text{ hours}$$

$$T = 9.9 \text{ hours}$$

APPENDIX III

SPECIFICATION FOR INFRARED RELAY OPTICS

1.0 General Description

This specification covers the final design and fabrication of a relay optical system for an infrared instrument designed to operate in the wavelength band from 10.5 to 12.5 microns. The relay system collects radiation which has been brought to focus by an f/1 Cassegrain-type telescope (the optical beam is modulated at this primary image location; the telescope is not a part of this procurement). The size of the primary image is 0.25 mm by 0.25 mm. The optical beam is first collimated by a germanium collimator lens (lenses), slightly focused by an f/8 lens and further focused by an aplanatic lens near the infrared detector. This is illustrated schematically in Figure III-1. The beam is collimated so that the separation between the collimator lens and the focusing lenses can be changed a moderate amount without affecting the over-all magnification of the relay system. The radii of curvature of the f/8 focusing lens and the aplanatic lens, their clear apertures, and their diameters have been calculated. Tolerances for the different radii and the quality of the refracting surfaces have not been established. These can be determined from the over-all performance requirements. The detailed design of the collimator lens (lenses) has not been determined, but calculations for a single germanium lens designed for minimum spherical aberration show that such a lens has too much residual aberration; it is felt that a doublet will give suitable performance.

All of the lenses shall have their refracting surfaces antireflection-coated for high transmission in the 10.5 to 12.5 micron band. The average transmission of each lens shall be 90 percent or more in this spectral band. The bandpass of 10.5 to 12.5 microns is established by an interference-type filter located just in front of the aplanatic lens (the optical filter is not a part of this procurement).

The over-all magnification of the relay system is 2X, i.e., the infrared detector has a sensitive area of 0.50 mm by 0.50 mm.

The performance requirements for the collimator lens assembly are given below. The configurations of the f/8 focusing lens and the aplanatic lens are also given. The aberrations of these latter two lenses have been calculated (assuming the radii of curvatures given) and show that satisfactory performance would be achieved if the given radii are sufficiently closely obtained in manufacture. The resolution requirements of the focusing lenses are given below as an aid in determining manufacturing tolerances.

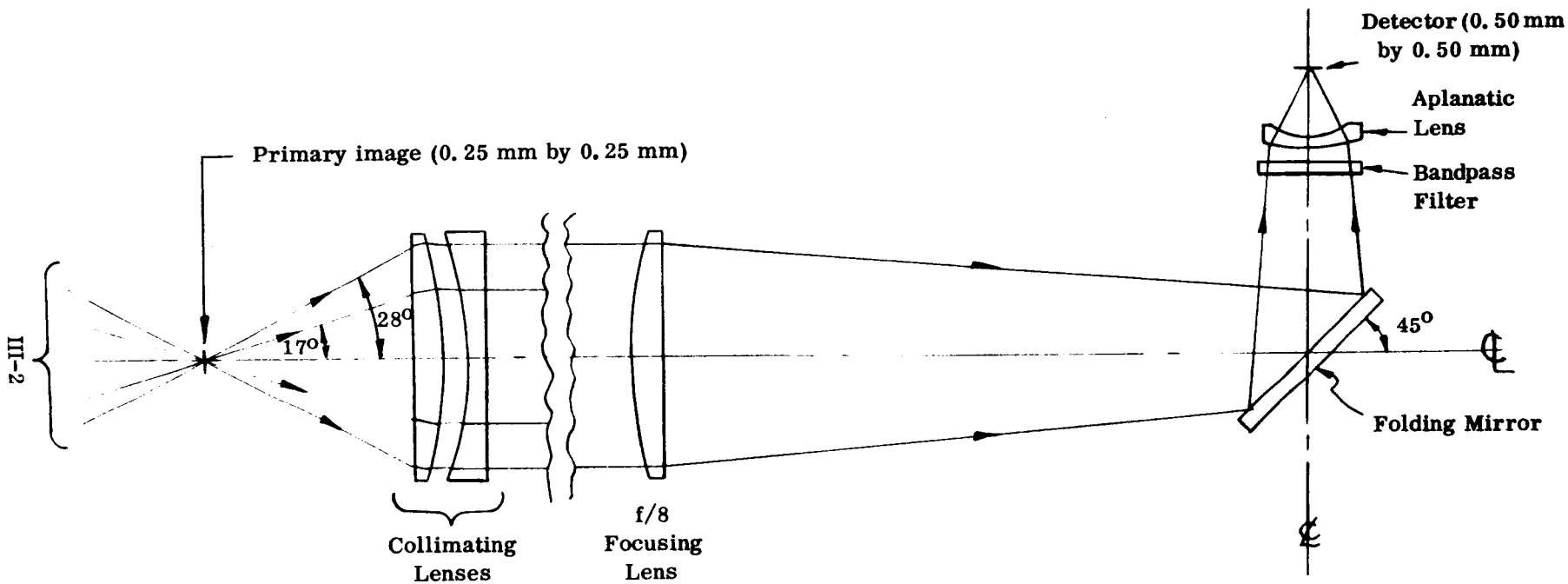

Figure III-1 Infrared Relay Optics (Not to Scale)

2.0 Collimator Lens

The collimator lens can be thought of as a telescope lens used in reverse. The resolution specified below would be for an input collimated beam with the optical rays traveling in the reverse direction from that in normal use. This lens (or lens assembly) shall meet the following requirements:

Focal length	1.25 inches
Clear aperture (collimated beam dia.)	1.35 inches
Effective aperture	1.25 inches
Lens diameter	1.500 ± 0.005 inches
Spot size in focal plane (for 10.5 to 12.5 micron radiation, 90 percent of energy)	1.5×10^{-3} inch or less
Lens material	Germanium
Antireflection coating	As specified in Section 1.0

3.0 Focusing f/8 Lens

This lens is drawn below and shall meet the following requirements:

Focal length	10.0 inches
Clear aperture (both surfaces)	1.40 inches
Effective aperture	1.25 inches
Lens diameter	1.500 ± 0.005 inches
Spot size (used singly)	4×10^{-3} inch or less
Lens material	Germanium
Antireflection coating	As specified in Section 1.0

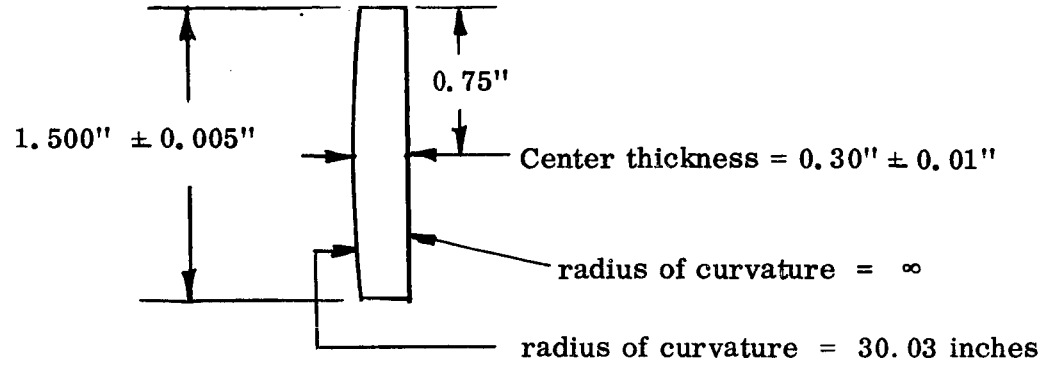

4.0 Aplanatic Lens

This lens is used to increase the "speed" of the optical beam and focus the radiation on the infrared detector. The requirements for the lens are given below and on the drawing:

Lens material	Germanium
Antireflection coating	As specified in Section 1.0
Spot size (when used in perfect f/8 beam)	1×10^{-3} inch or less at detector

5.0 Mounting

The lens elements will be mounted by ITT Industrial Laboratories. Appropriate location or spacing information for the collimator lenses must be supplied to ITTIL. No information is required for mounting of the f/8 or aplanatic focusing lenses.

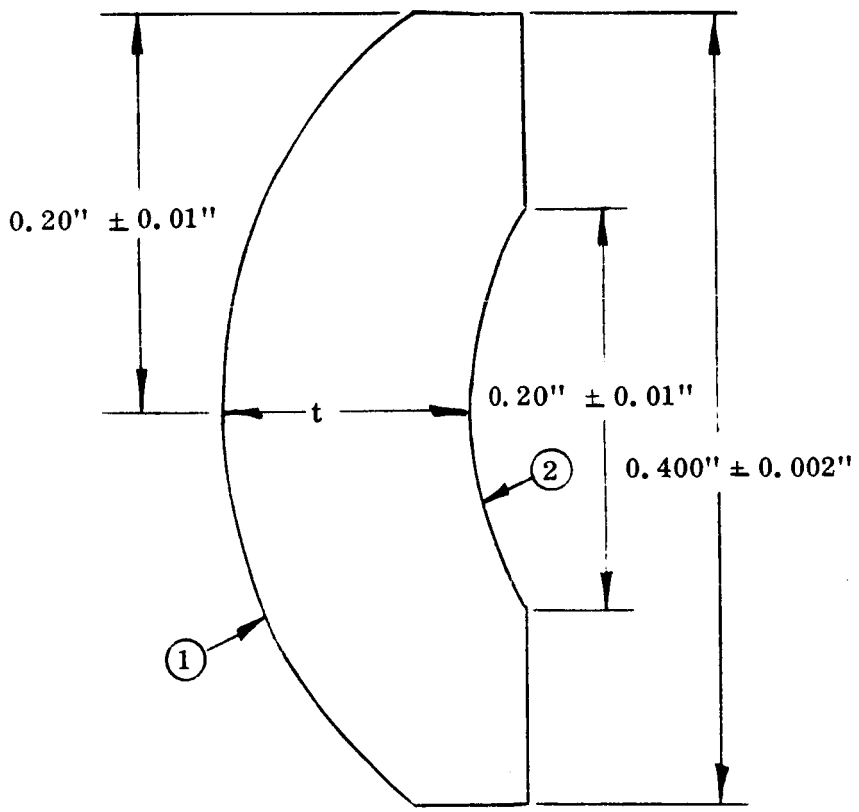

Radius of curvature of surface 1 = 6.40 mm (millimeters)

Radius of curvature of surface 2 = 4.80 mm

Center thickness = t = 3.20 mm

Clear aperture of surface 1 = 0.32" ± 0.01"

Clear aperture of surface 2 = 0.20" ± 0.01"

Material - germanium

Scale = approximately 10X

APLANATIC LENS